Supporting Information

Nanomolar Level Detection of Chemotoxic [UO2]2+ Ions by a Free Carboxylate Anchored Metal-Organic Framework

*Sk Sakir Hossain and Shyam Biswas**

[a] Department of Chemistry, Indian Institute of Technology Guwahati, 781039, Assam, India.

*Corresponding author. Tel: 91-3612583309

E-mail address: sbiswas@iitg.ac.in

Materials and Characterization Methods:

All of the chemicals were purchased from commercial suppliers and used directly without further purification. The 2-(carboxymethoxy)terephthalic acid (H_3L) was prepared according to the below mentioned procedure. The Attenuated Total Reflectance Infrared (ATR-IR) spectra were recorded using PerkinElmer UATR Two at the ambient condition in the region 400-4000 cm^{-1}. The notations used for characterization of the bands are broad (br), strong (s), very strong (vs), medium (m), weak (w) and shoulder (sh). Fluorescence sensing studies were performed with a HORIBA JOBIN YVON Fluoromax-4 spectrofluorometer. Fluorescence lifetimes were measured using Picosecond Time-resolved and Steady State Luminescence Spectrometer on an Edinburg Instruments Lifespec II & FSP 920 instrument. A Bruker Avance III 600 NMR spectrometer was used for recording ^1H and ^{13}C NMR spectra at 400 and 500 MHz, respectively. The mass spectrometry of the synthesized linker was obtained with Ultra-High Performance Liquid Chromatograph - Quadrupole Time of Flight - High Resolution Mass Spectrometer (UHPLC-QTOF-HRMS, Agilent G6546A). Thermogravimetric analysis (TGA) was carried out with a Netzsch STA-409CD thermal analyzer in the temperature range of 30-700 °C in an O_2 atmosphere at the heating rate of 4 °C min^{-1}. PXRD data were collected by using Rigaku Smartlab X-ray diffractometer with Cu-Kα radiation (λ = 1.54056 Å), 40 kV of operating voltage and 125 mA of operating current. N_2 sorption isotherms were recorded by using Quantachrome Quadrasorb evo volumetric gas adsorption equipment at -196 °C. Before the sorption analysis, the degassing of the compound was carried out at 100 °C under a high vacuum for 24 h. Gemini 500 was utilized for energy dispersive X-rays spectrometer (EDX) for elemental characterization. FE-SEM images were captured with a Zeiss (SIGMA 300) scanning electron microscope. FE-TEM image was captured with a JEOL Field Emission - Transmission electron microscope. XPS measurements were performed with PHI-5000 Versaprobe III (ULVAC-PHI Inc.) using He(I) (21.22eV) excitation. Pawley refinement was carried out using Materials Studio software.

Preparation of MOF (1') Suspension for Fluorescence Sensing Experiments:

The sensing experiments were performed in aqueous medium for both the analytes. The aqueous suspension of the MOF was prepared as follows. At first, 1 mg of probe **1'** was suspended in a glass vial containing 4 mL of water and placed in a sonication bath for 30 min. After that the vial was kept overnight at room temperature to make the suspension stable. The fluorescence sensing experiment was executed using 300 µL of the above-mentioned suspension in a quartz cuvette containing 3 mL of distilled water. The fluorescence data were recorded upon exciting the suspension at 310 nm. For competitive analysis, different analyte solutions (10 mM) were added to the above suspension and the emission response was recorded.

Calculation of Standard Deviation (σ):

The σ value was calculated using the six blank readings of MOF suspension (1583630, 1583650, 1567590, 1579650, 1580170, and 1575120) by using equation S1:

$\sigma = \sqrt{\Sigma(xi - \mu)^2/N}$ ……..equation S1

Where, 'x_i' is the fluorescence intensities of the blank readings of MOF suspension,

'µ' is the mean of the blank reading

'N' is the number of blank readings.

The obtained value of standard deviation using the above formula is 758.5, which is further utilized for the calculation of LOD, as discussed in the main manuscript.

Table S1. Calculation of standard deviation.

x_i	μ	$x_i - \mu$	$(x_i - \mu)^2$	$\Sigma(x_i - \mu)^2$	$\Sigma(x_i - \mu)^2/N$	$\sqrt{\Sigma(x_i - \mu)^2/N}$
1583630	1578301.667	5328	28387584	187167284	31194547	5585
1583650		5348	28601104			
1567590		-10712	114746944			
1579650		1348	1817104			
1580170		1868	3489424			
1575120		-3182	10125124			

Quantum Yield Measurement:

Here, we have utilised the Parker-Rees method to calculate the quantum yield of the prepared MOF, using a 0.5 M H_2SO_4 solution of quinine sulphate as a standard reference.[1] The formula for this calculation is provided as follows:

$$\Phi_s = (A_r F_S n_s^2 / A_s F_r n_r^2) \Phi_r \quad \text{.....(Equation-1)}$$

In this equation, Φ_r represents the quantum yield of the quinine sulphate reference solution, while Φ_s represents the quantum yield of the sample. The values of A_r and A_s correspond to the absorbance of the reference and sample, respectively, whereas F_r and F_s refer to the integrated area of fluorescence intensity for the reference and sample, respectively. The refractive indices of the reference and sample are represented by n_r and n_s, respectively. Table S1 contains the relevant photophysical parameters and quantum yield values.

Table S2. Photophysical parameters of quinine sulphate and **1'** are required for quantum yield calculation of **1'**.

Sl. No.	Sample Name	Excitation Wavelength λ_{ex} (nm)	Absorbance (A)	Area of Integrated Fluorescence Intensity (F)	Quantum Yield (Φ)
1	quinine sulphate	310	0.054	2.25E8	0.546
2	**1'**	308	0.160	5.47E7	0.044
3	**1'** after treatment with uranyl	308	0.212	3.17E7	0.019

Synthesis of 2,5-bis(Carboxymethoxy)Terephthalic Acid (H_4L Linker):

The linker was synthesized in four steps (Scheme S1). In first step, 2-hydroxyterephthalic acid was synthesized from 2-aminoterephthalic acid by following the reported literature.[2] After that, the esterification of 2-hydroxy terephthalic acid was performed with the help of earlier reported lieature.[3] In the third step, 590 mg (2.8 mmol) of dimethyl 2-hydroxyterephthalate was dissolved in 15 mL of acetonitrile in a 50 mL round-bottom flask. Then, 370 µL (3.5 mmol) of methyl bromoacetate and 580 mg (4.2 mmol) of potassium carbonate were added to the solution. Finally, the mixture was heated at 80 °C for 24 h under stirring condition. After completion of the reaction, the solvent was removed by evaporation under reduced pressure. After that the product was collected by solvent extraction method from dichloromethane-water mixture. Yield: 737 mg (2.6 mmol, 93%). The obtained product (737 mg, 2.6 mmol) was then further dissolved in 15 mL of tetrahydrofuran (THF). Then, 785 mg of NaOH was added to it (dissolved in 40 mL of water). Afterwards, the reaction mixture was heated at 70 °C for 24 h with continuous stirring. After the reaction was completed, THF was evaporated, and the aqueous phase was acidified with dilute HCl to get the solid compound. Finally, the product was collected by filtration and dried in a hot air oven. Yield: 450 g (1.9 mmol, 73%). The obtained product was characterized with ^{1}H NMR, ^{13}C NMR and HR-MS analysis (Figures S1-S3).

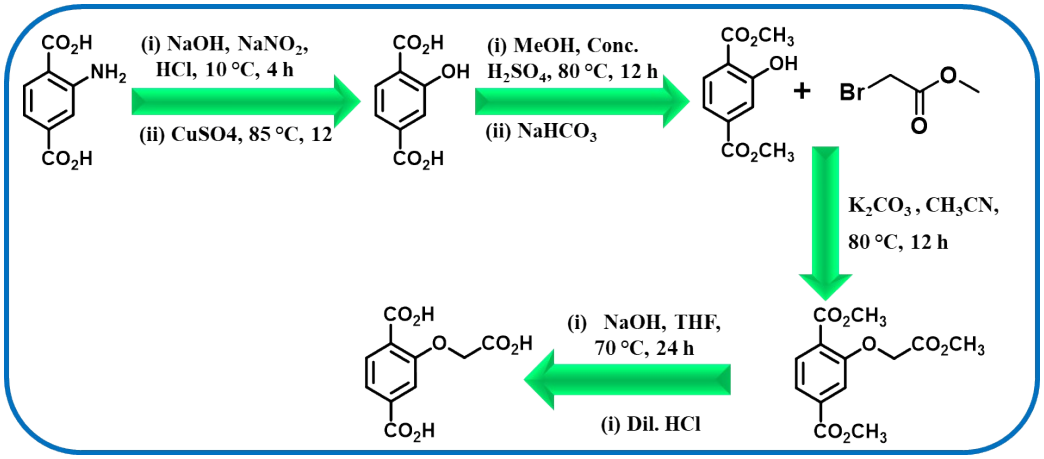

Scheme S1. Schematic representation for synthesis of H_3L linker.

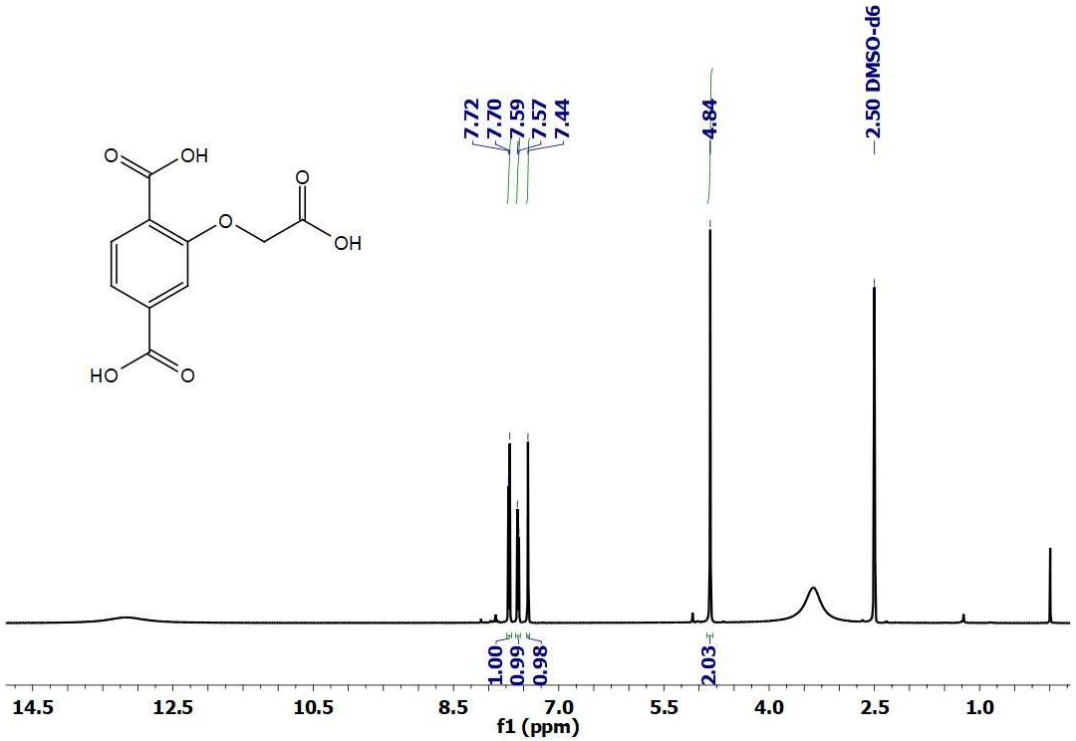

Figure S1. ^{1}H NMR spectrum (400 MHz, DMSO-d_6) of H_3L linker.

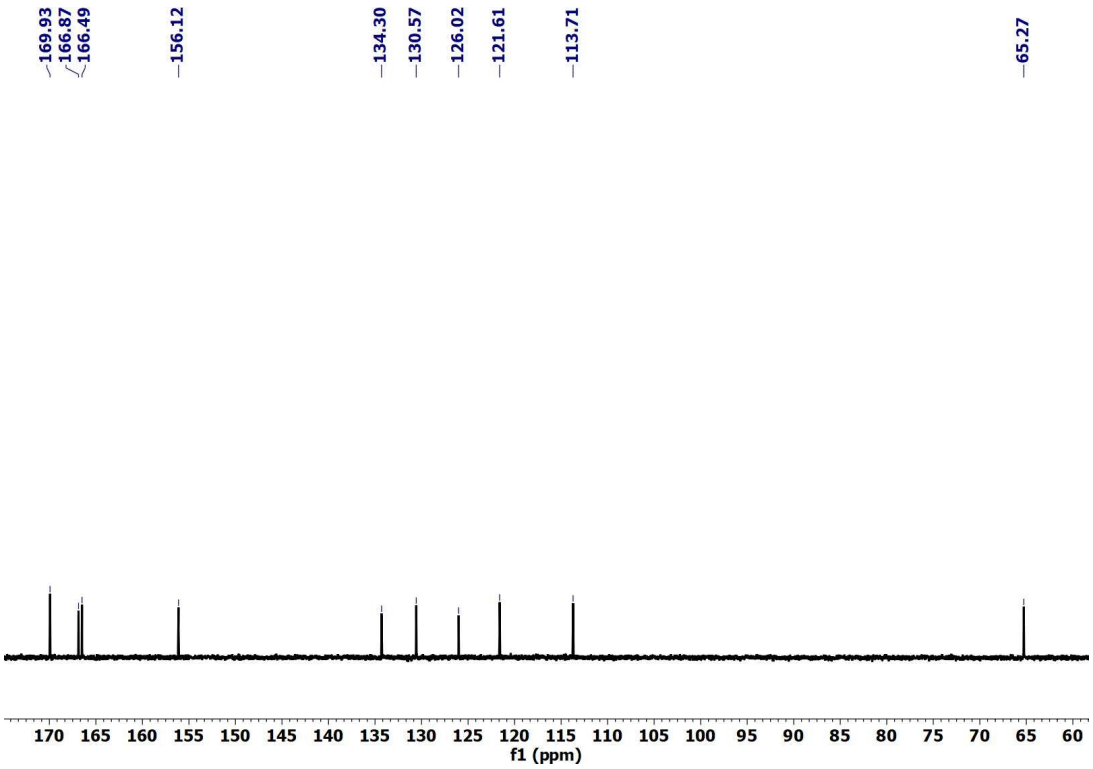

Figure S2. ^{13}C NMR spectrum (125 MHz, DMSO-d_6) of H_3L linker.

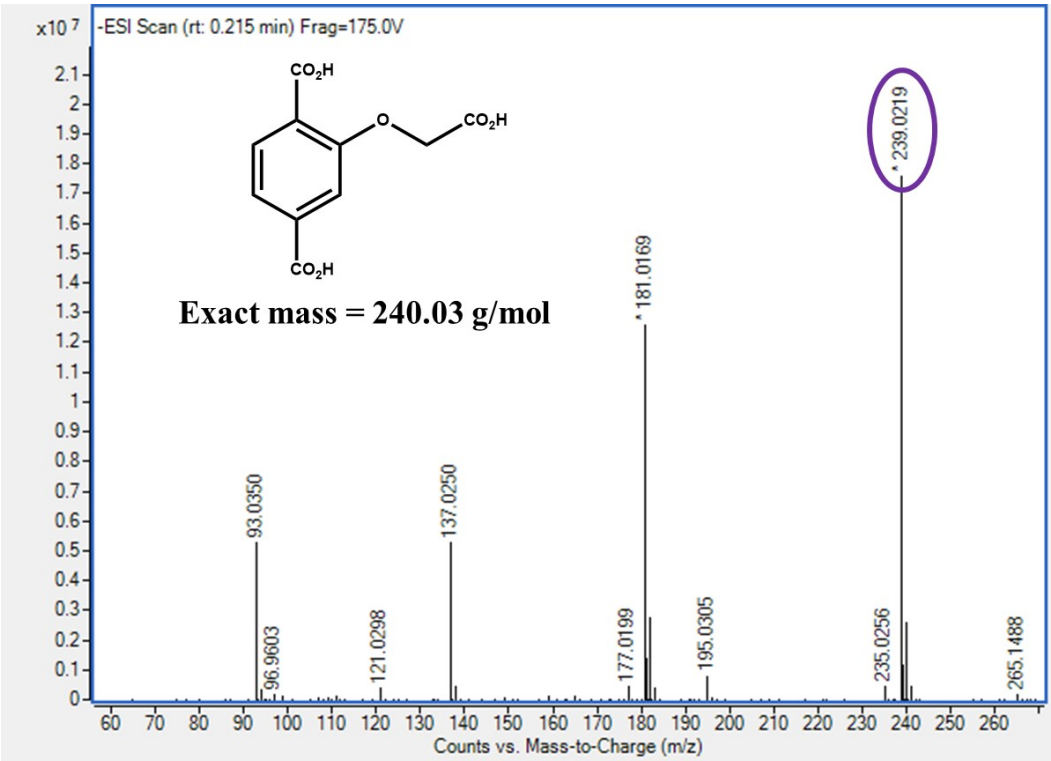

Figure S3. ESI-MS spectrum of H_2L linker measured in methanol. The spectrum shows m/z peak at 239.0219, which corresponds to $(M-H)^-$ ion (M = mass of 2,5-bis(carboxymethoxy)terephthalic acid linker).

Table S3. Indexing parameters of UiO-66 and synthesized **1**.

Compound Name	$[Zr_6O_4(OH)_4(C_{10}H_5O_7)_6]\cdot 15H_2O\cdot 2.5DMF$ (**1**) (this work)	UiO-66 (reported)[4]
Crystal System	Cubic	Cubic
a = b = c (Å)	20.7828 (11)	20.7004(2)
α = β= γ (°)	90	90
V (Å3)	8976.8 (8)	8870.3(2)

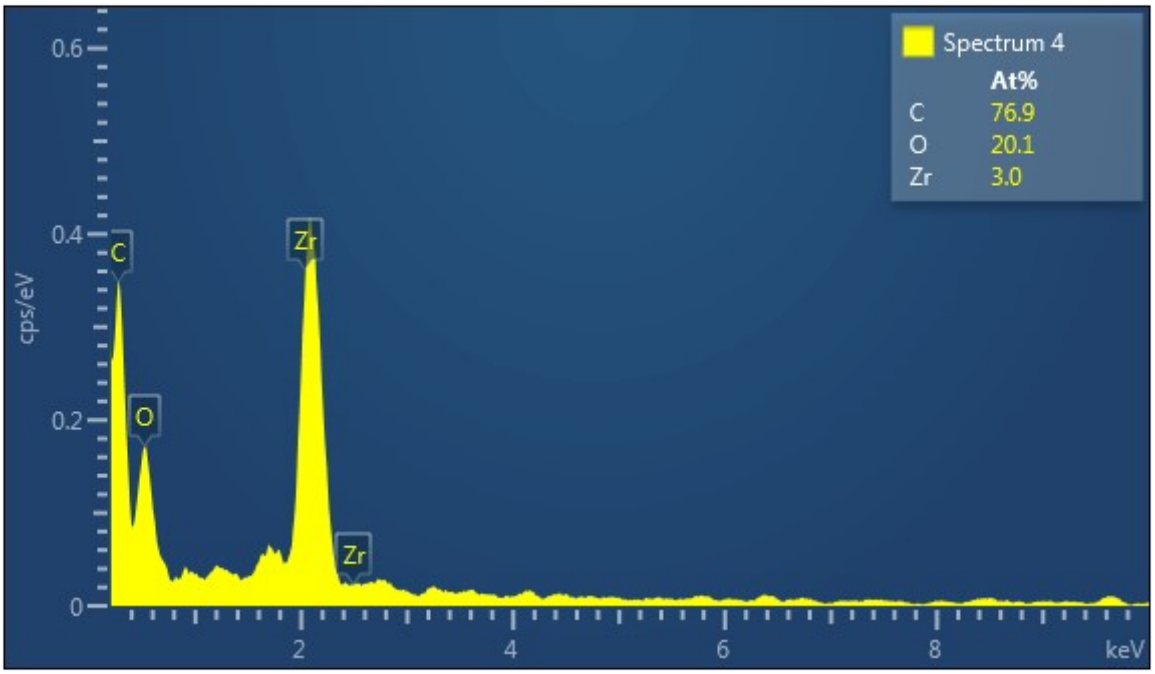

Figure S4. EDX spectrum of **1'**.

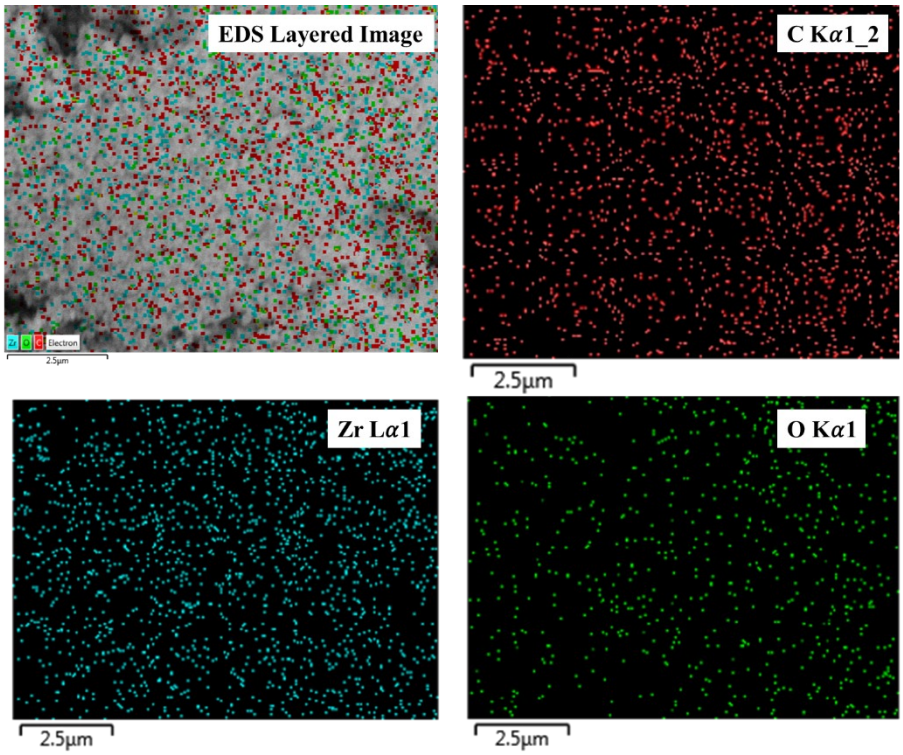

Figure S5. EDX elemental mapping of the elements present in **1'**.

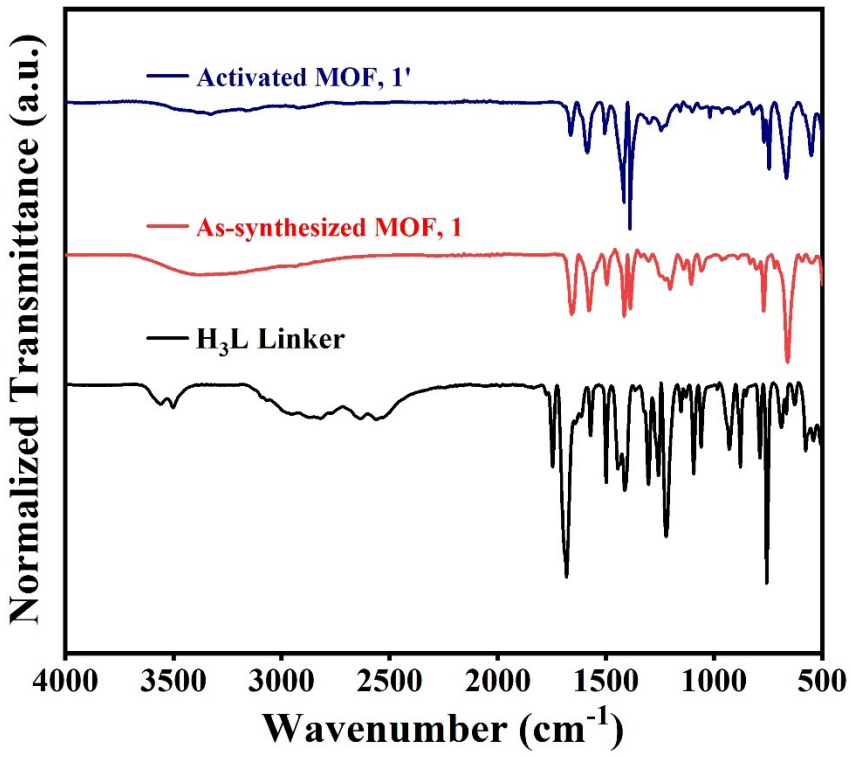

Figure S6. ATR-IR spectra of **1** and **1'** compared with the spectrum of the linker.

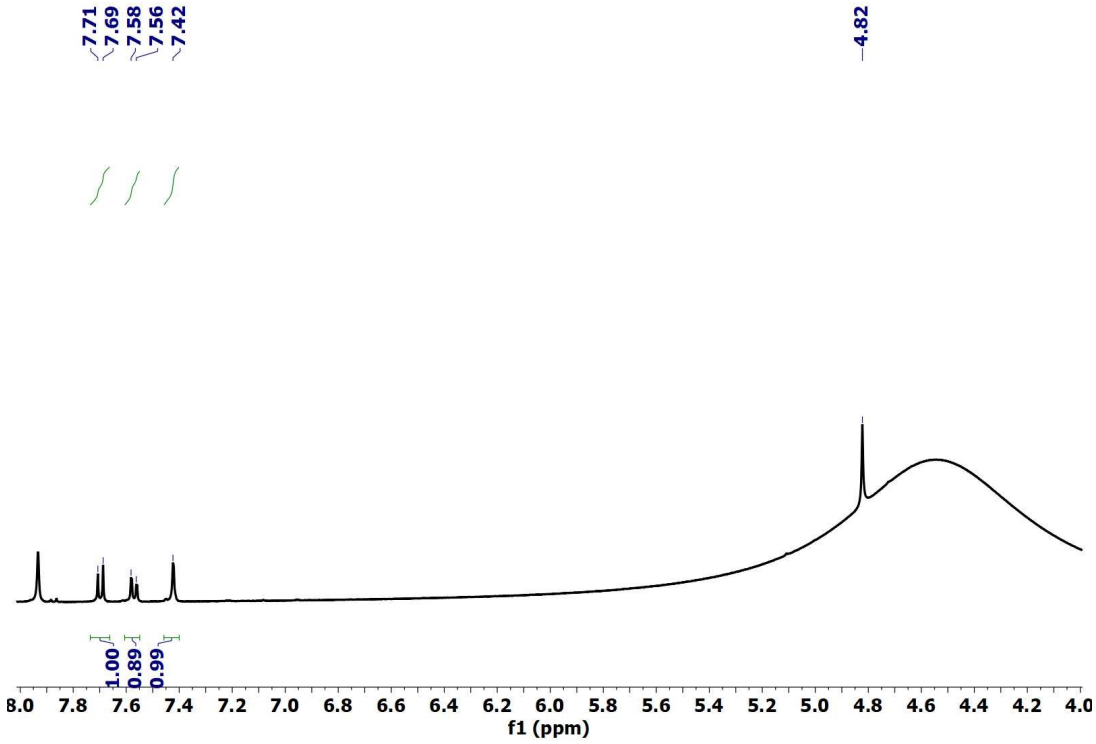

Figure S7. ^{1}H NMR spectrum (400 MHz, DMSO-d_6) of the digested **1** (digested with 40% aqueous solution of HF in DMSO-d_6).

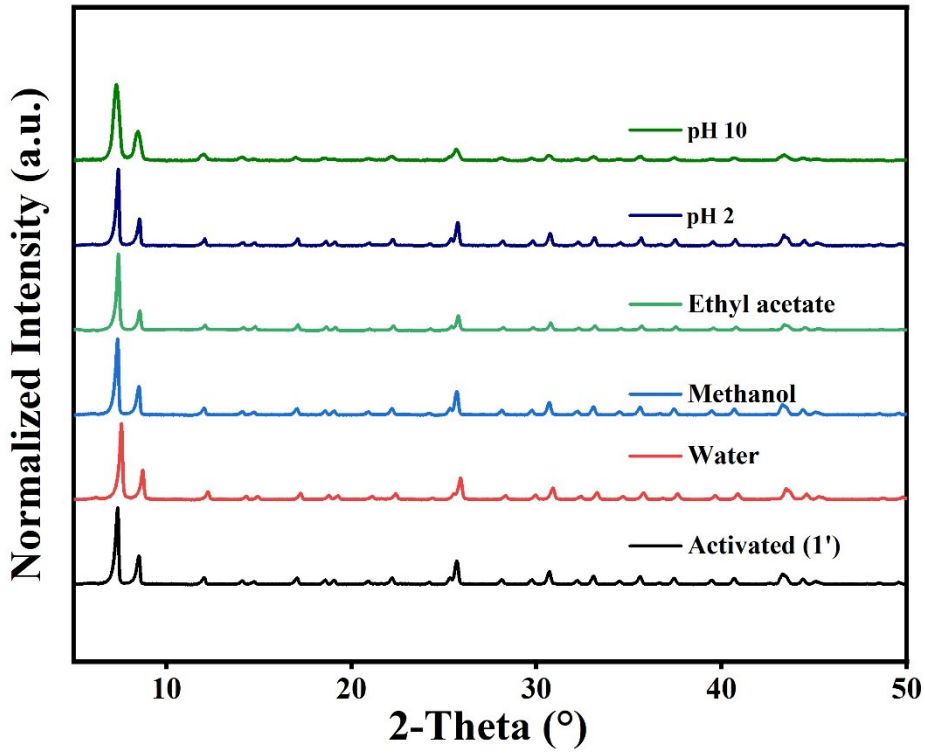

Figure S8. PXRD profiles of **1'** after stirring in different media for 24 h at room temperature.

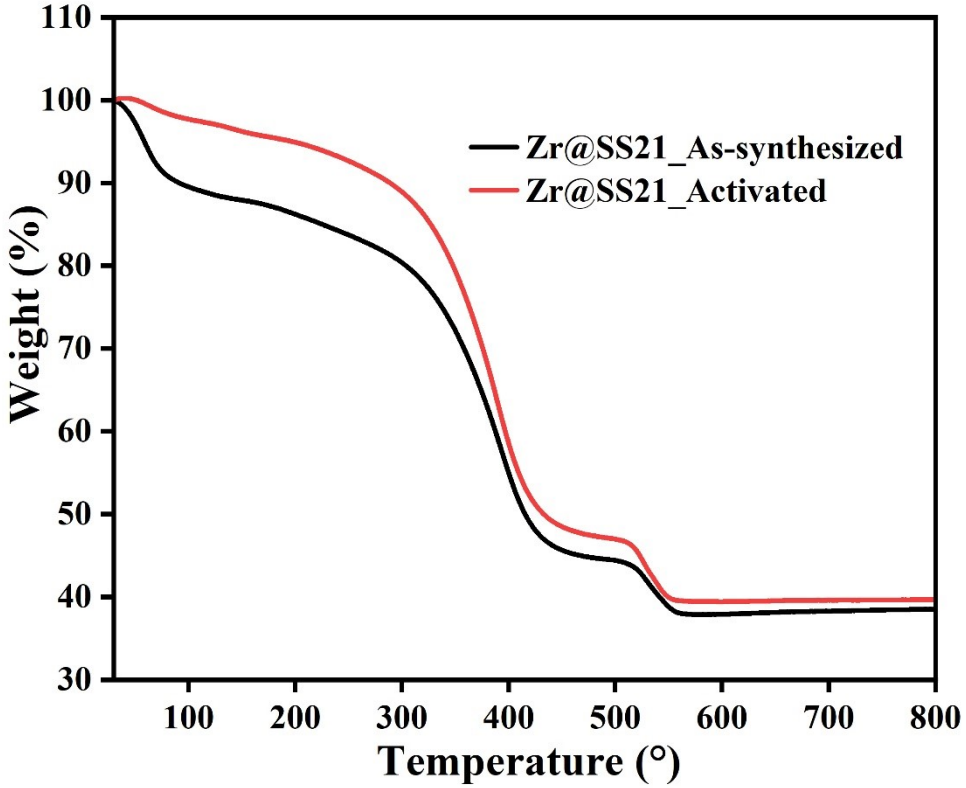

Figure S9. TGA curves of **1** and **1'** recorded under O_2 atmosphere in the temperature range of 30 °C to 800 °C with a heating rate of 4 °C/min.

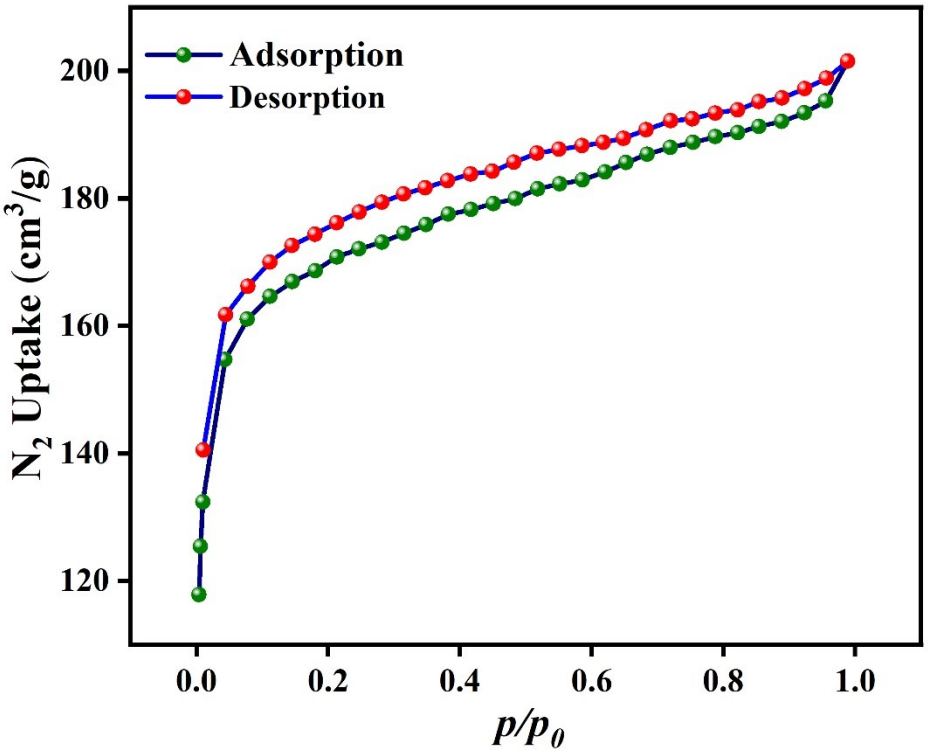

Figure S10. N_2 adsorption isotherms of **1'** measured at -196 ℃.

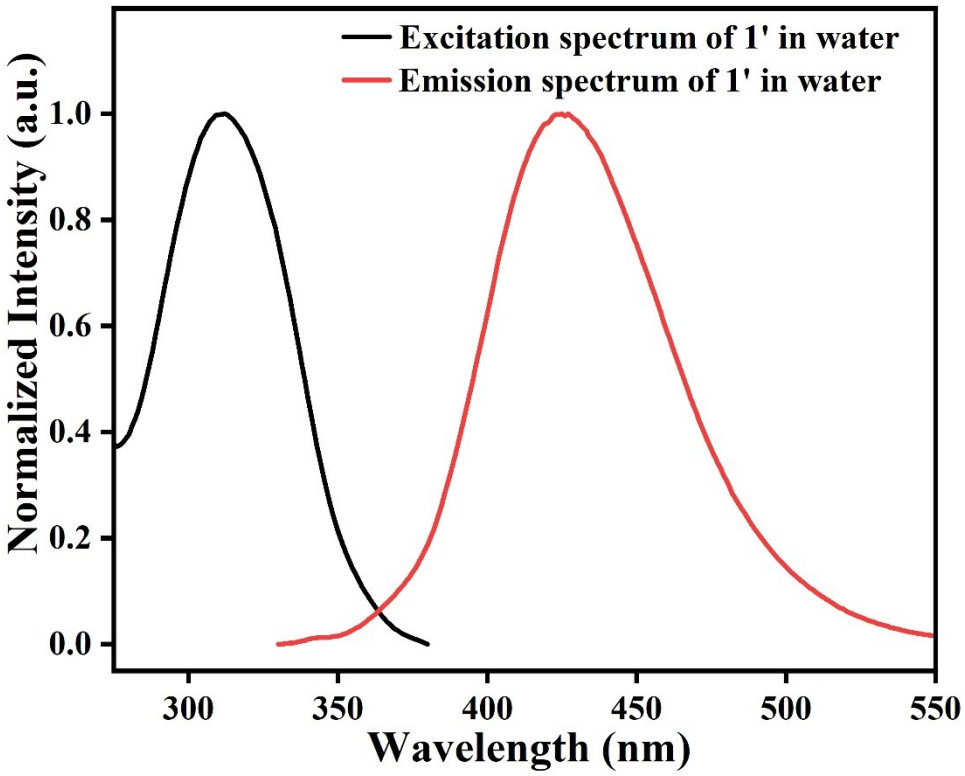

Figure S11. Fluorescence excitation and emission spectra of **1'** in water.

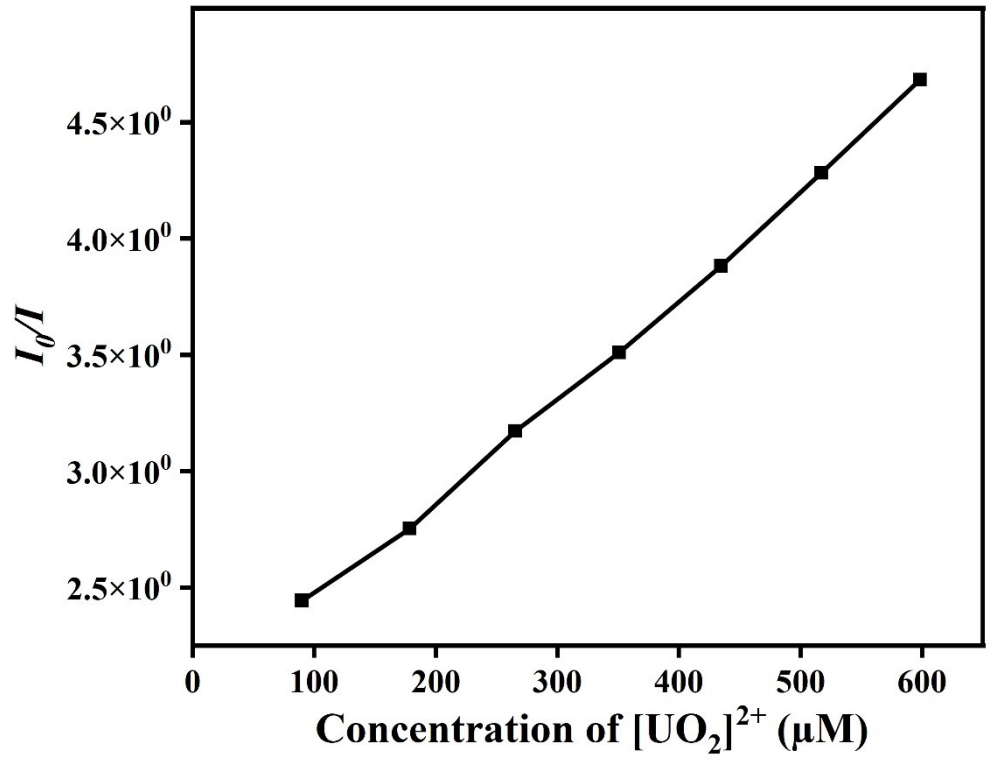

Figure S12. Stern-Volmer plot for fluorescence quenching of **1'** in the presence of $[UO_2]^{2+}$ in aqueous medium.

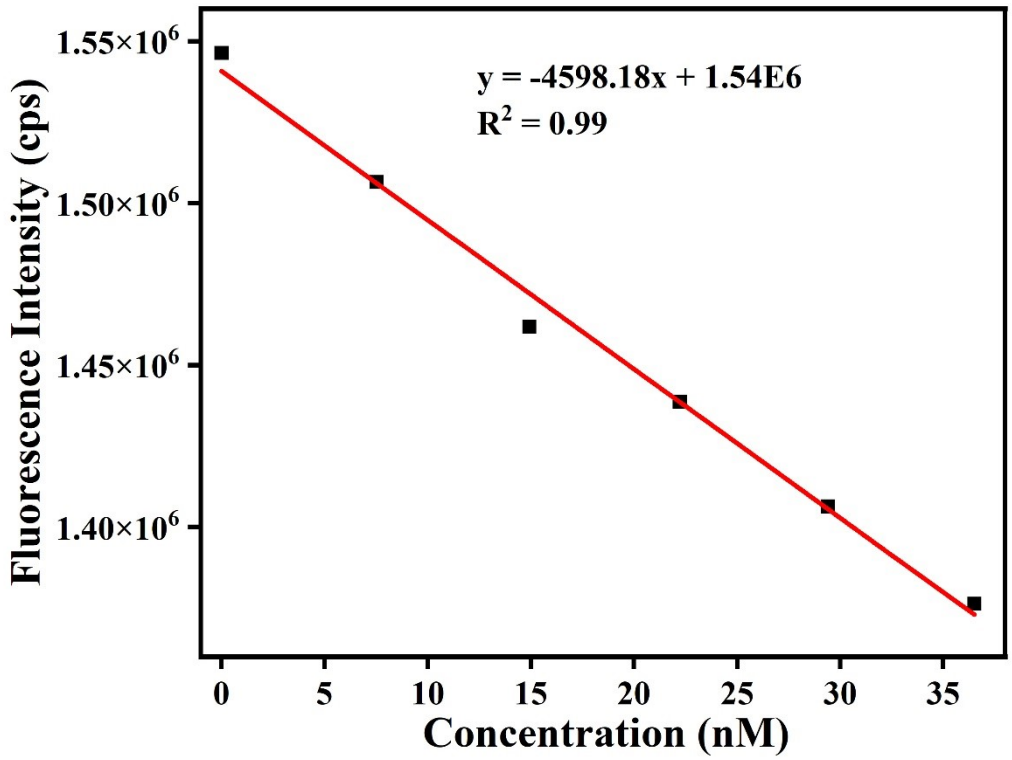

Figure S13. Change in fluorescence intensity of **1'** in water as a function of $[UO_2]^{2+}$ concentration.

Table S4. Comparison of the K_{SV}, detection limit, and response time for uranyl detection by **1′** with those of reported MOF-based fluorometric sensors.

Sl. No.	MOF-based fluorometric sensor	Quenching efficiency Constant (K_{SV}, M^{-1})	LOD (nM)	Reference
1	Tb@UiO-66-$(COOH)_2$	2.16×10^5	8 nM	5
2	DUT-101	1.03×10^4	35	6
3	Eu-MOF	8.40×10^4	90	7
4	YTU-100	8.10×10^4	4.5	8
5	Zn-MOF	4×10^4	400	9
6	[Co2(dmipm)(nda)2]n	1.01×10^4	13.2 µM	10
7	[Zn(HBTC)(BMIOPE)· DMF·H_2O]n	2.29×10^4	24.7 µM	11
8	FA@ZIF-8	-	5	12
9	**$[Zr_6O_4(OH)_4(C_{10}H_6O_7)_6]$ (1')**	**3.34×10^6**	**3.2**	**this work**

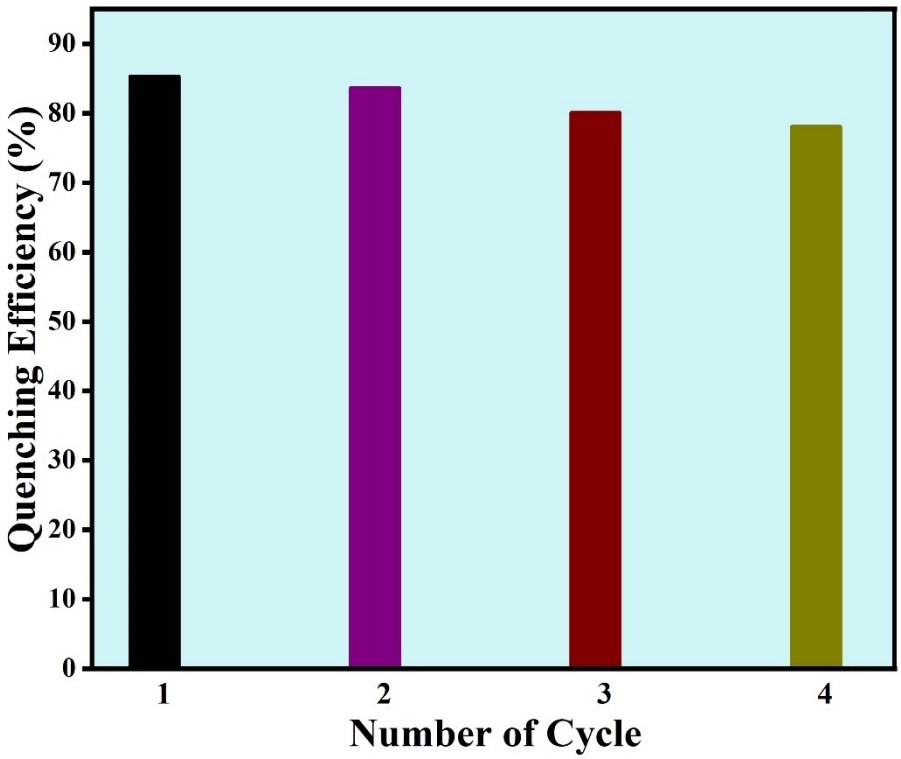

Figure S14. Reusability of **1'** for $[UO_2]^{2+}$ sensing in aqueous medium.

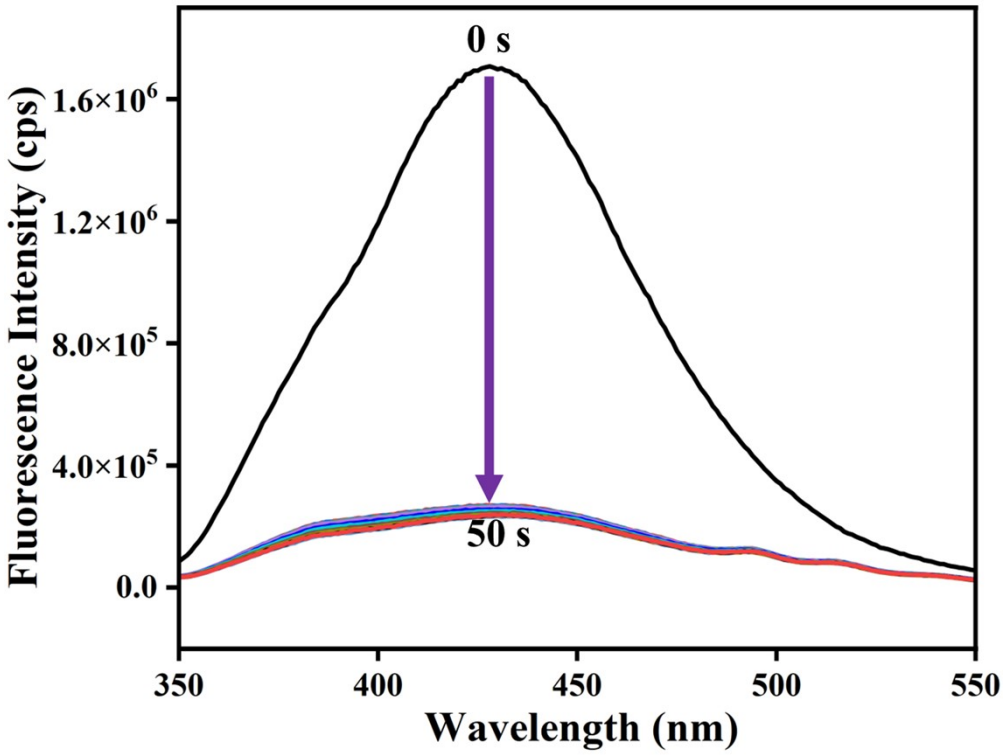

Figure S15. Volume-dependent quenching study for fluorometric sensing of $[UO_2]^{2+}$ by **1'** in aqueous medium (fluorescence data were recorded at 5 s time interval up to 50 s).

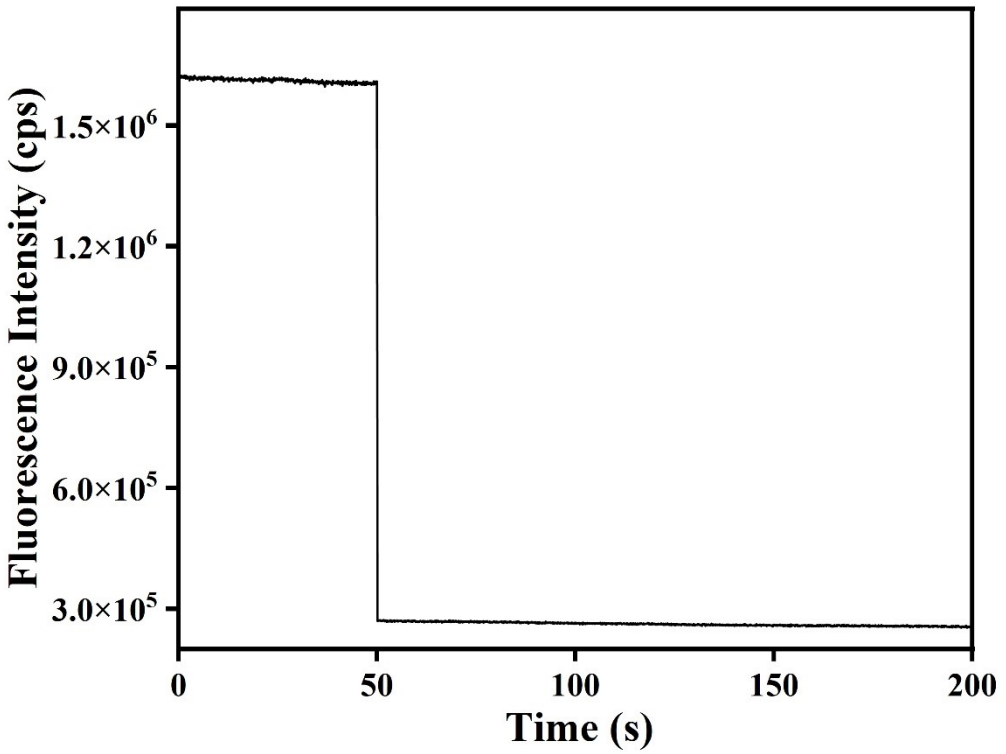

Figure S16. Fluorometric kinetic study for sensing of $[UO_2]^{2+}$ by **1'** in aqueous medium.

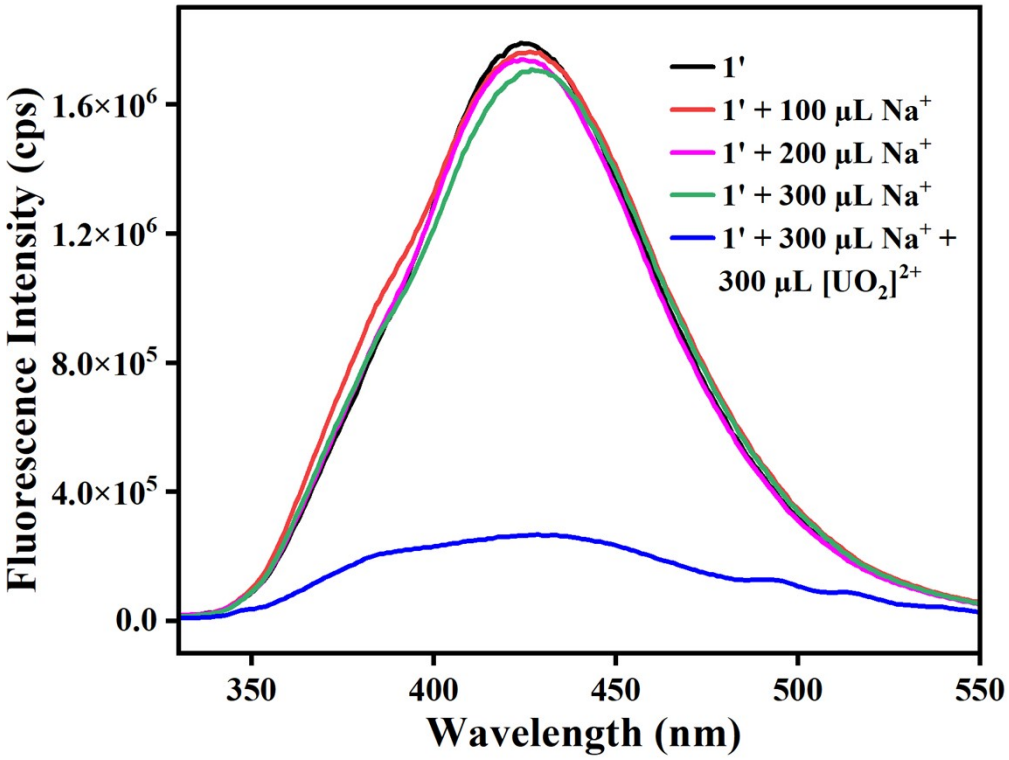

Figure S17. Selective detection of $[UO_2]^{2+}$ in fluorometric turn-off mode by **1′** in presence of Na^+ in aqueous medium.

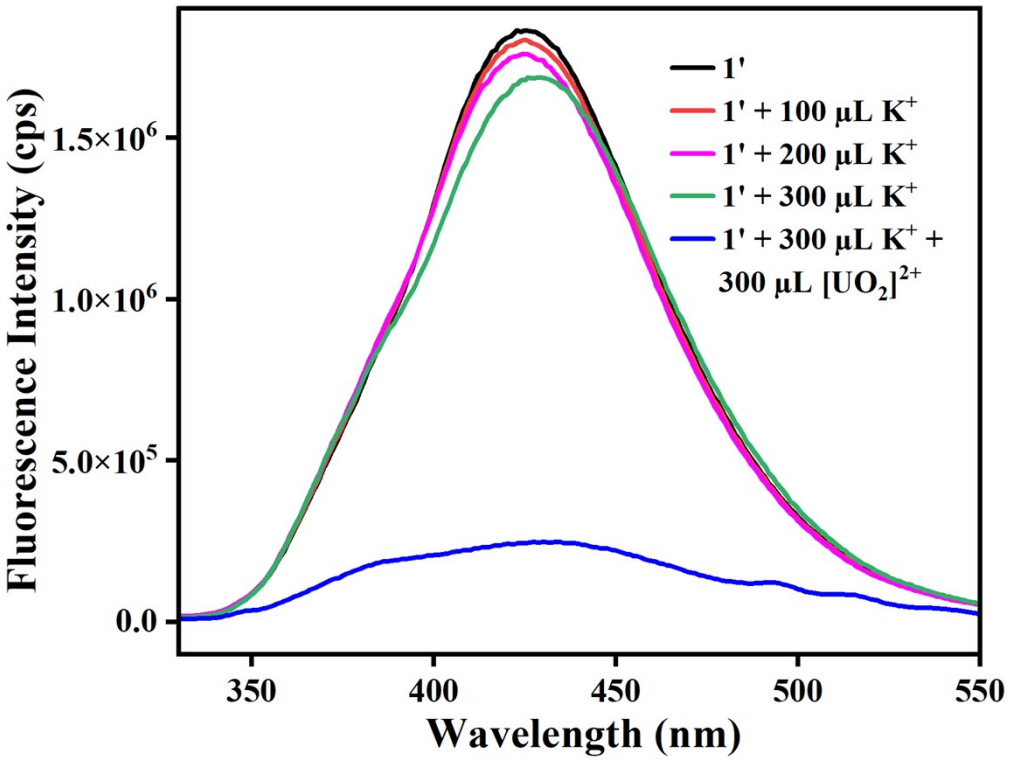

Figure S18. Selective detection of $[UO_2]^{2+}$ in fluorometric turn-off mode by **1′** in presence of K^+ in aqueous medium.

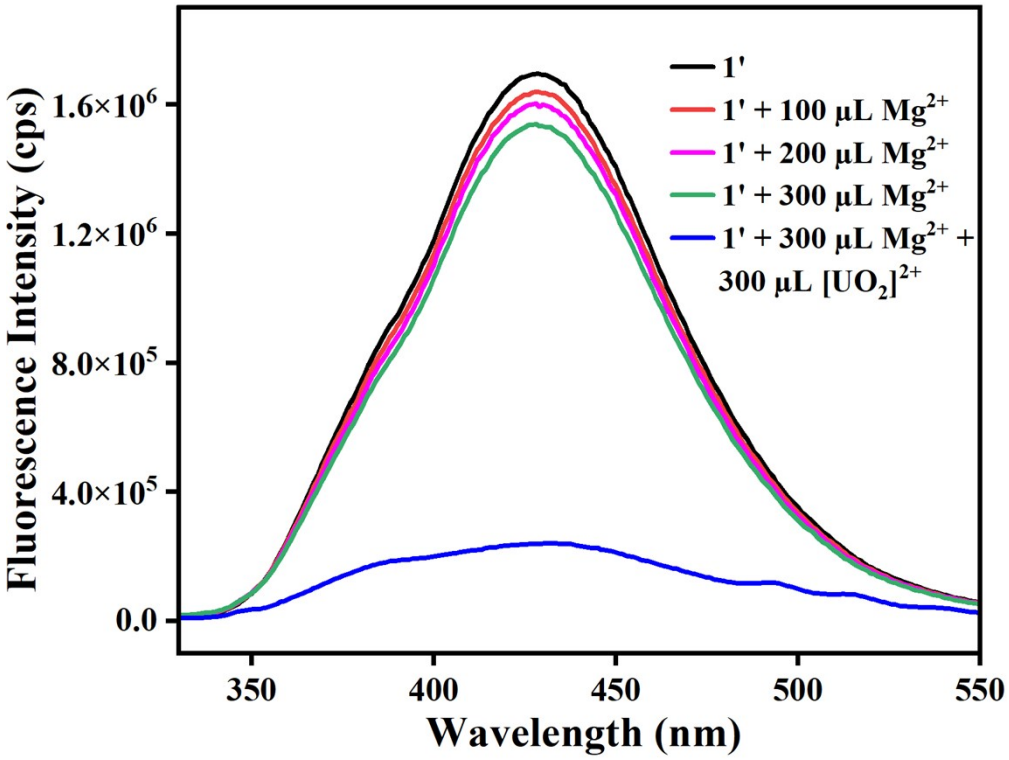

Figure S19. Selective detection of $[UO_2]^{2+}$ in fluorometric turn-off mode by **1′** in presence of Mg^{2+} in aqueous medium.

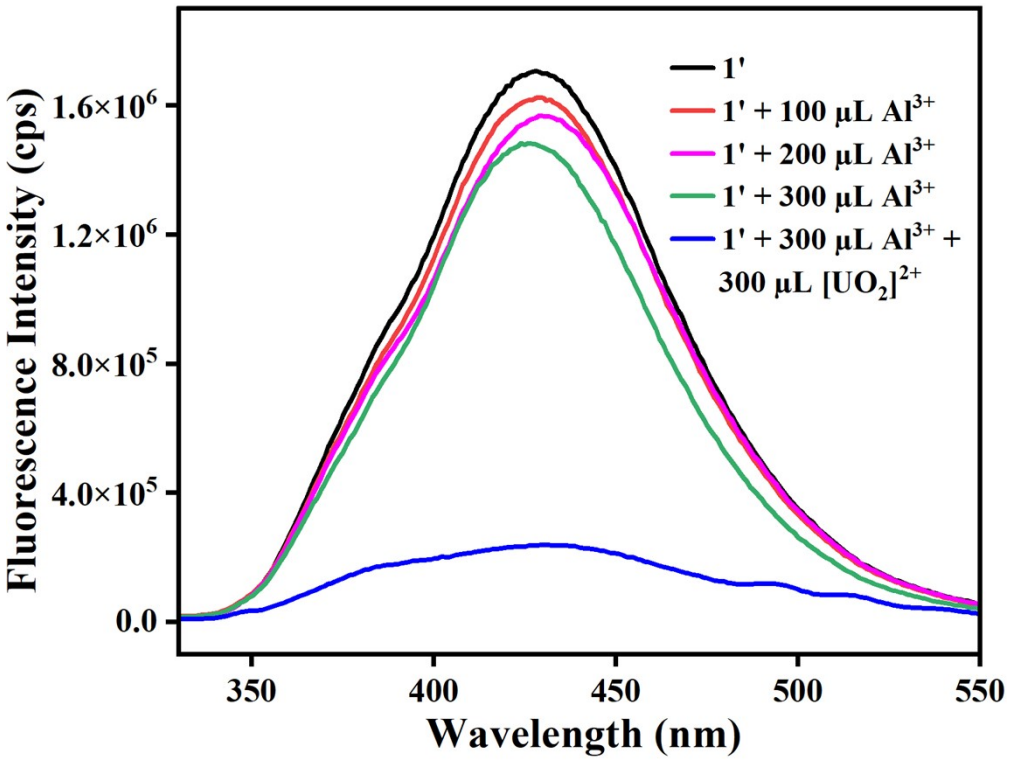

Figure S20. Selective detection of $[UO_2]^{2+}$ in fluorometric turn-off mode by **1′** in presence of Al^{3+} in aqueous medium.

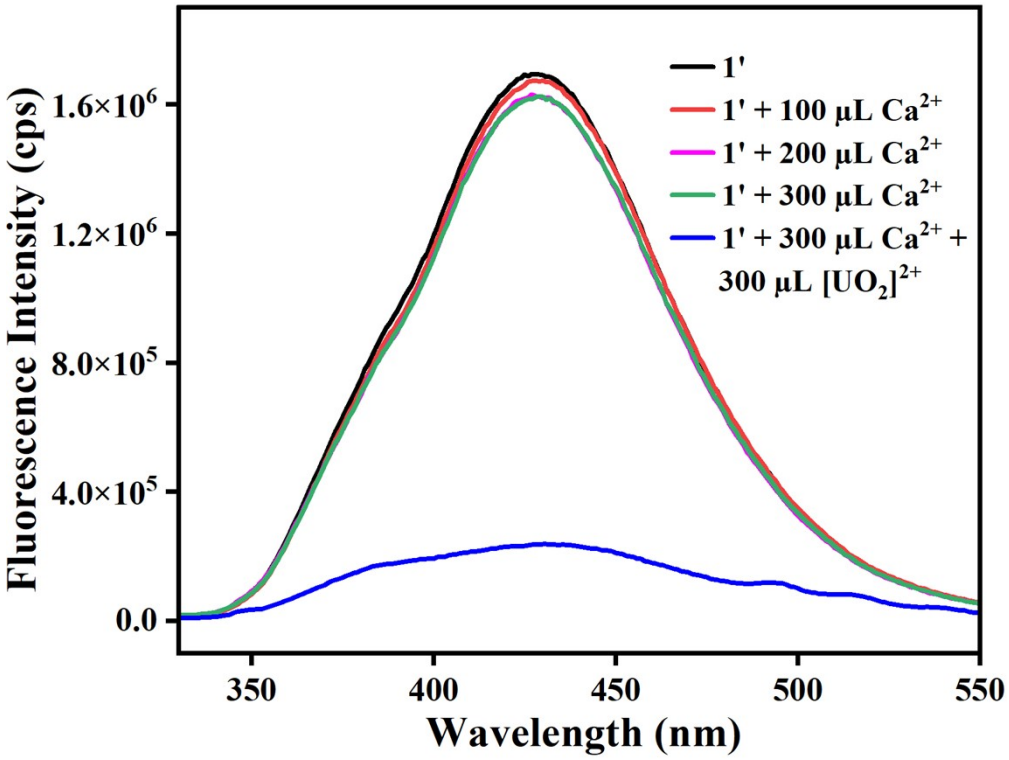

Figure S21. Selective detection of $[UO_2]^{2+}$ in fluorometric turn-off mode by **1′** in presence of Ca^{2+} in aqueous medium.

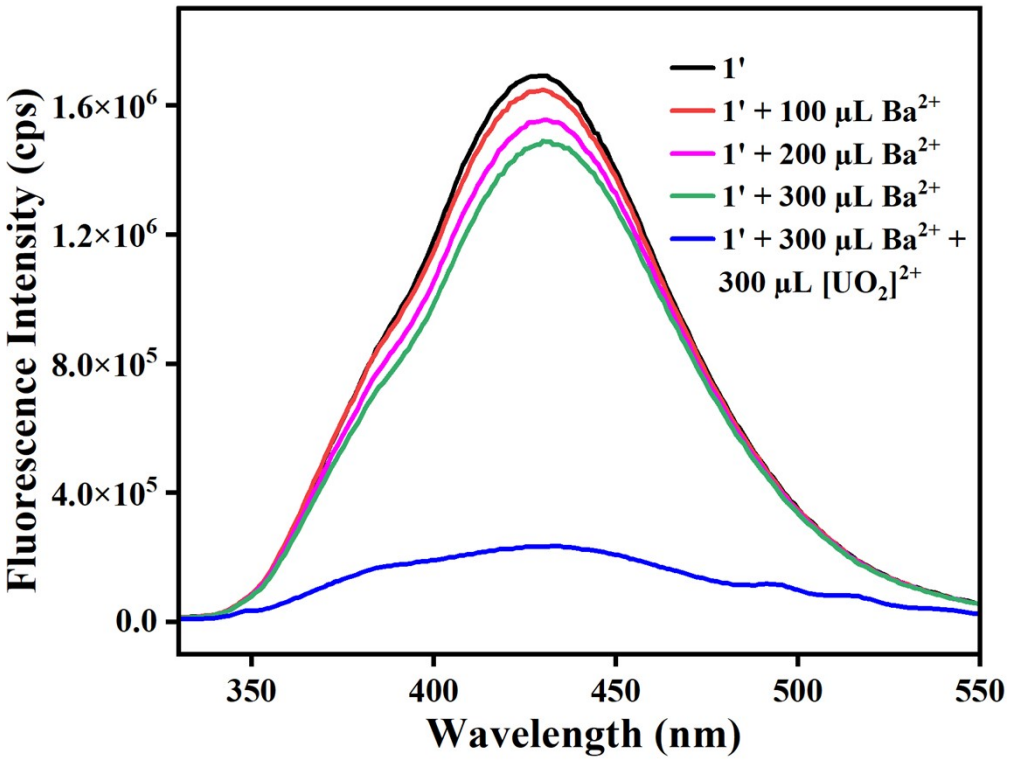

Figure S22. Selective detection of $[UO_2]^{2+}$ in fluorometric turn-off mode by **1′** in presence of Ba^{2+} in aqueous medium.

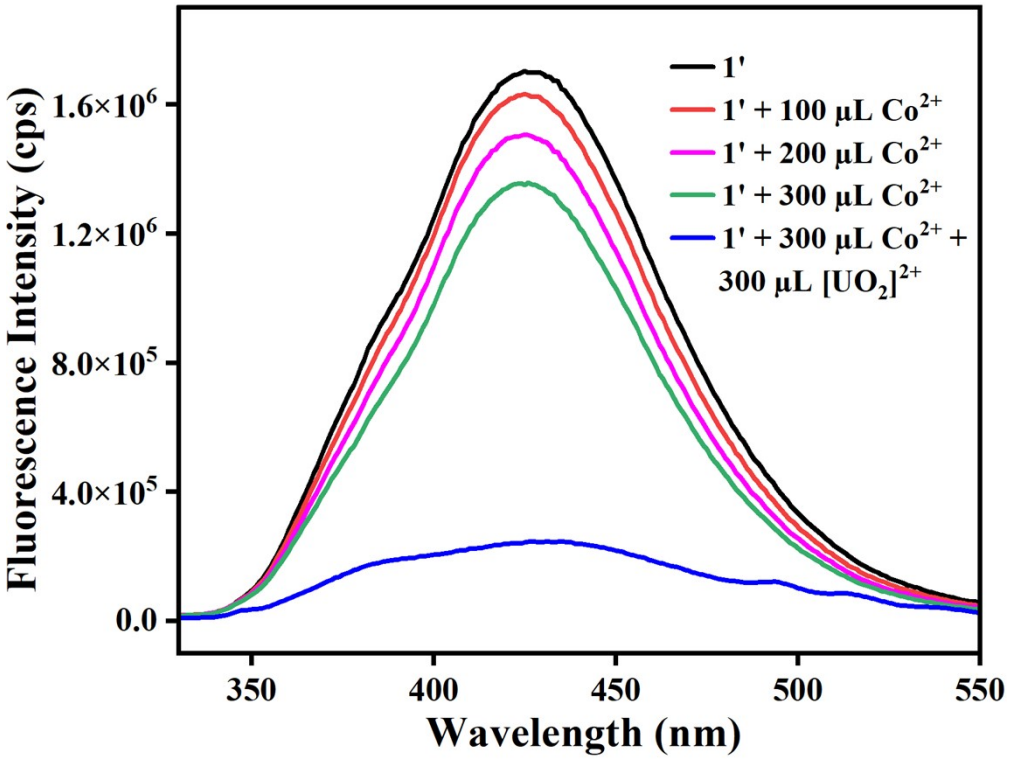

Figure S23. Selective detection of $[UO_2]^{2+}$ in fluorometric turn-off mode by **1′** in presence of Co^{2+} in aqueous medium.

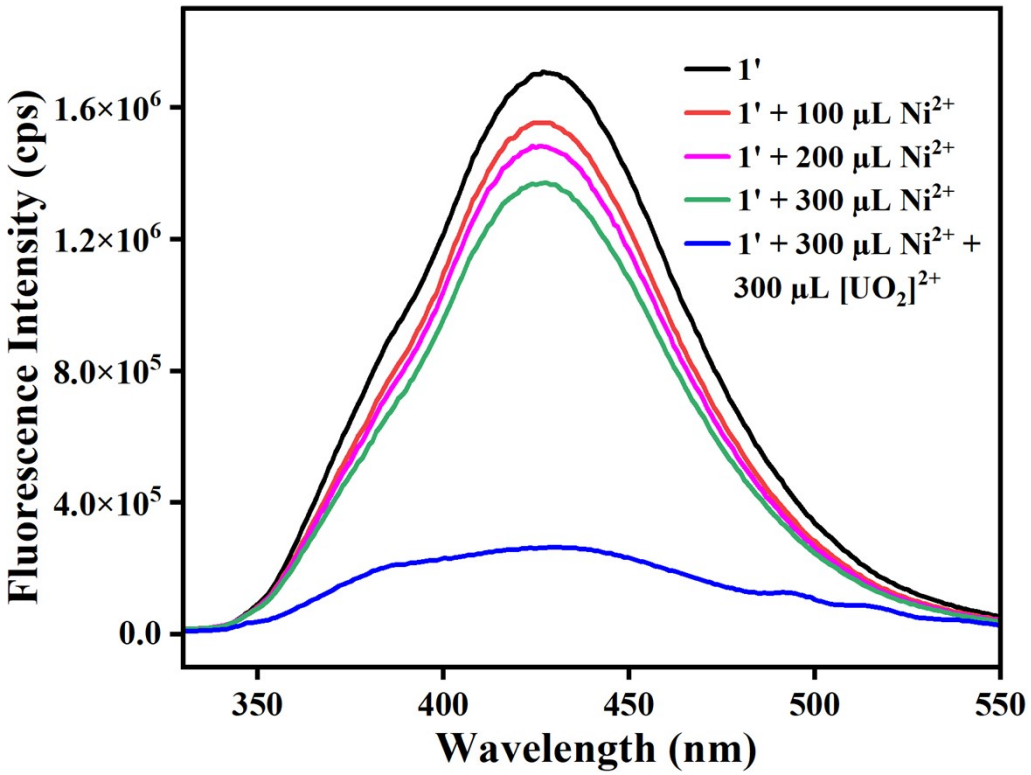

Figure S24. Selective detection of $[UO_2]^{2+}$ in fluorometric turn-off mode by **1′** in presence of Ni^{2+} in aqueous medium.

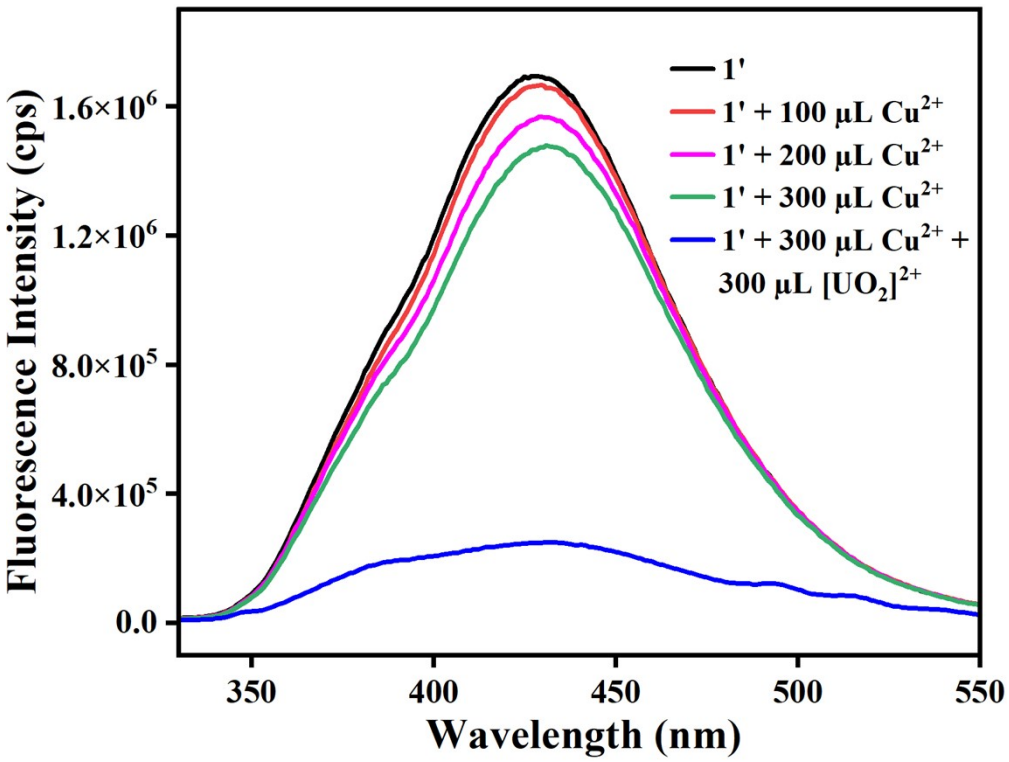

Figure S25. Selective detection of $[UO_2]^{2+}$ in fluorometric turn-off mode by **1′** in presence of Cu^{2+} in aqueous medium.

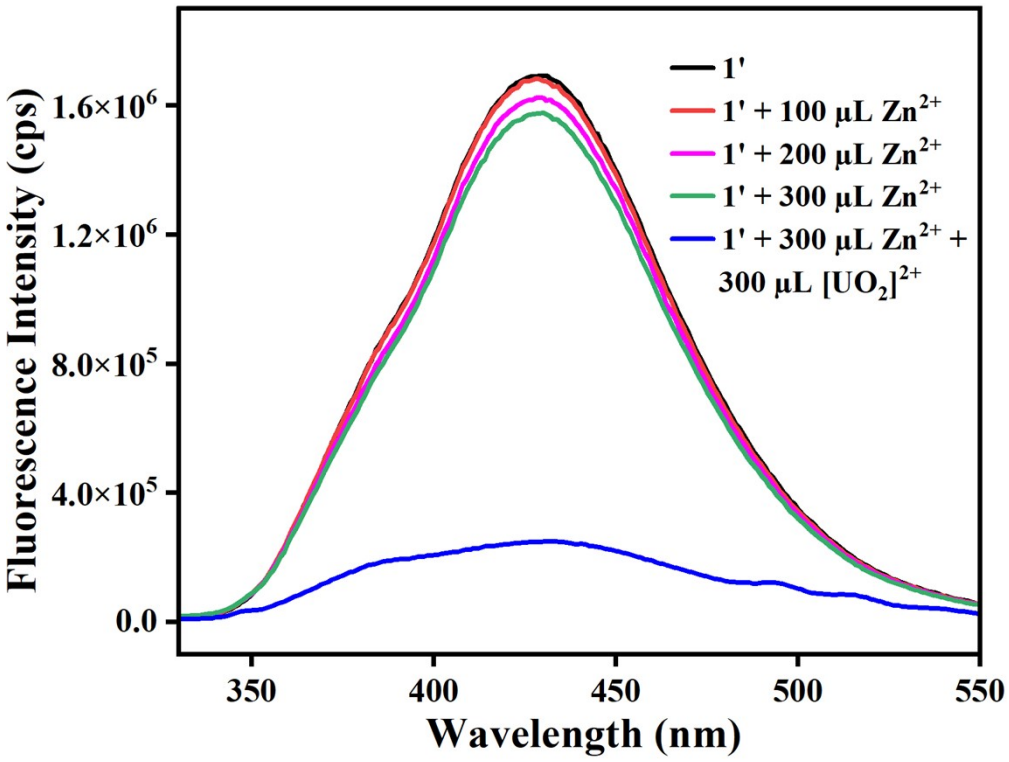

Figure S26. Selective detection of $[UO_2]^{2+}$ in fluorometric turn-off mode by **1′** in presence of Zn^{2+} in aqueous medium.

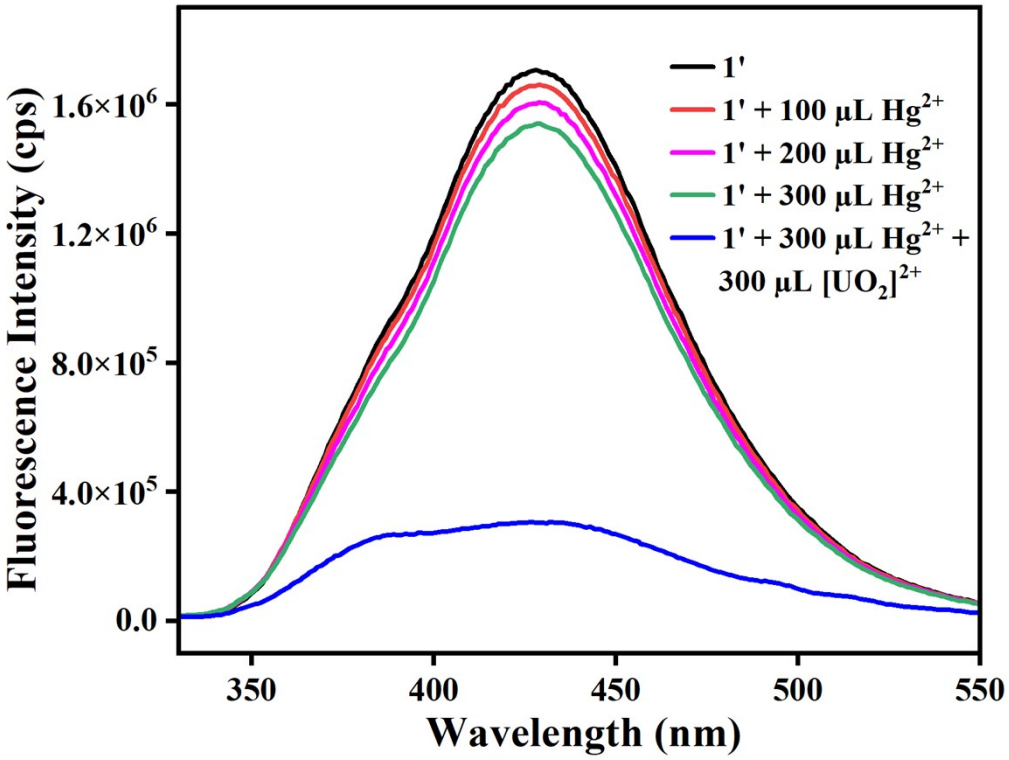

Figure S27. Selective detection of $[UO_2]^{2+}$ in fluorometric turn-off mode by **1′** in presence of Hg^{2+} in aqueous medium.

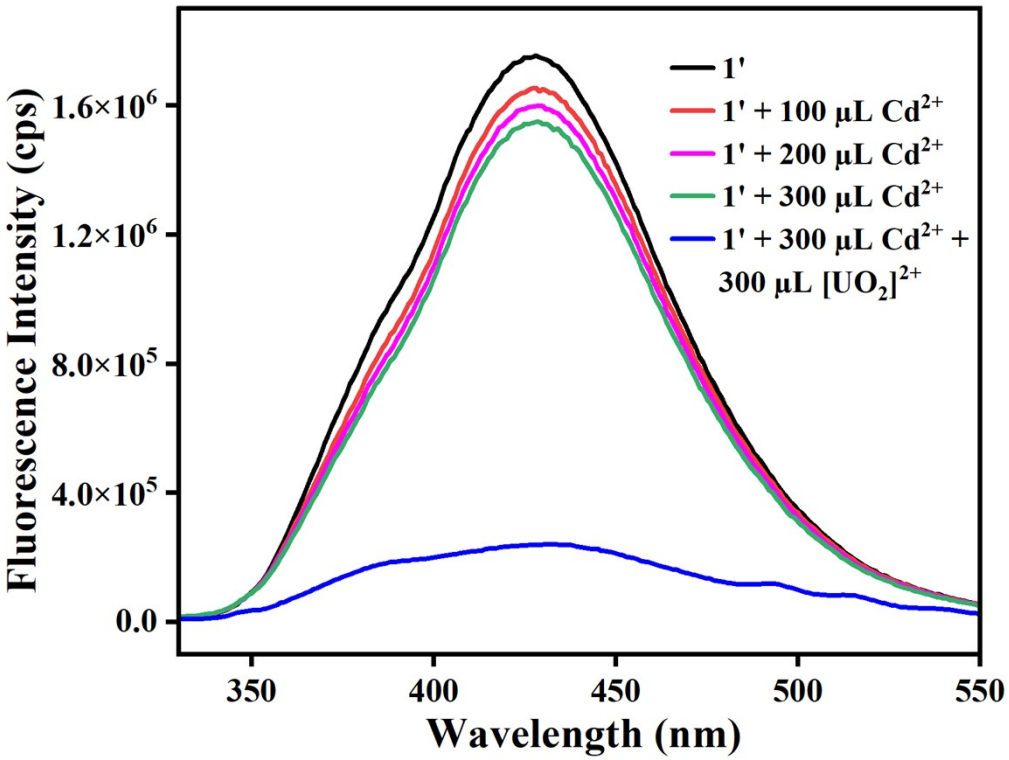

Figure S28. Selective detection of $[UO_2]^{2+}$ in fluorometric turn-off mode by **1′** in presence of Cd^{2+} in aqueous medium.

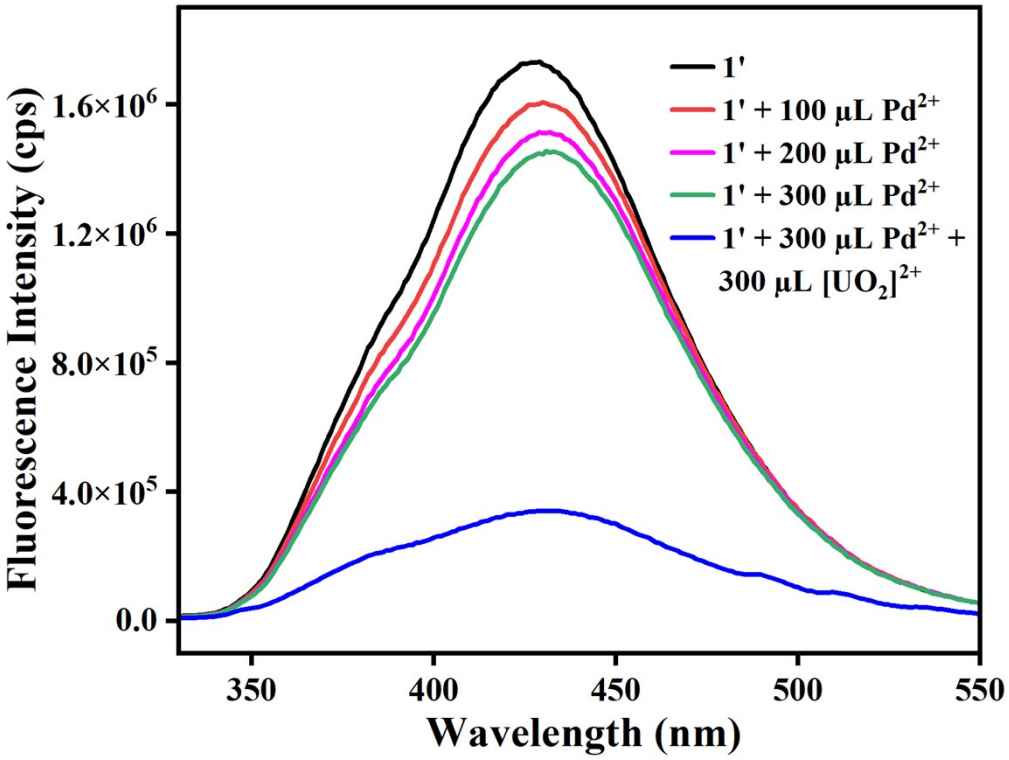

Figure S29. Selective detection of $[UO_2]^{2+}$ in fluorometric turn-off mode by **1′** in presence of Pd^{2+} in aqueous medium.

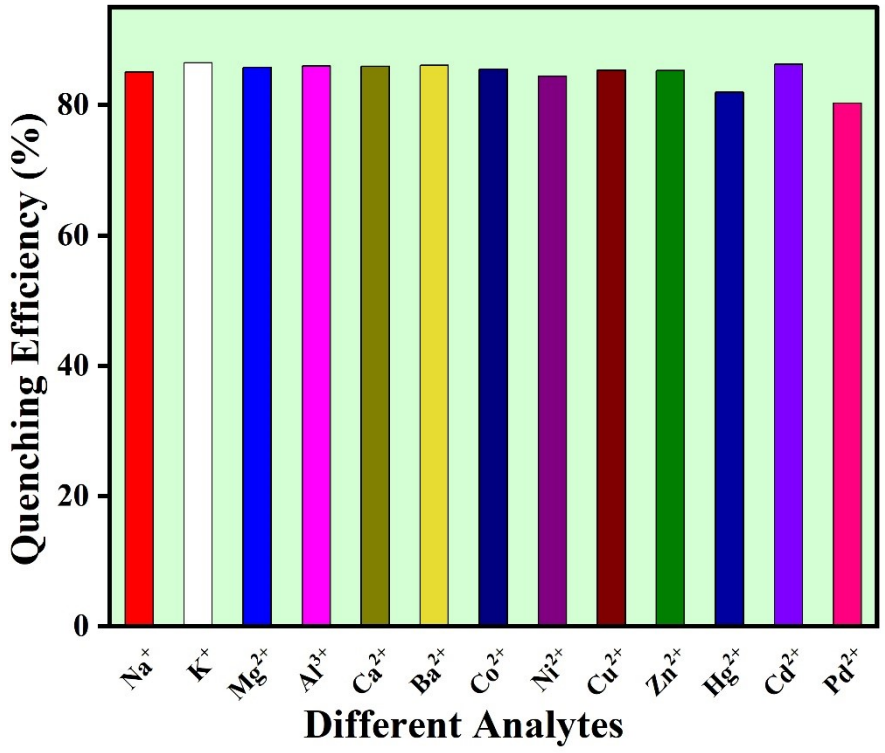

Figure S30. Quenching efficiency of $[UO_2]^{2+}$ in the presence of different interfering analytes in aqueous medium (10 mM aqueous solution of each analyte).

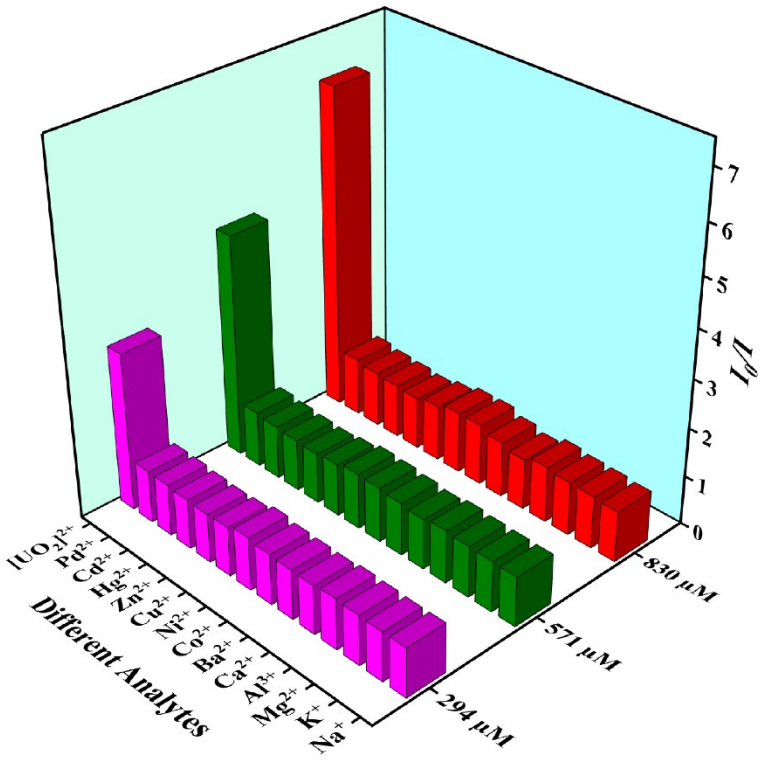

Figure S31. Three-dimensional S-V plot for $[UO_2]^{2+}$ sensing by **1′** in aqueous medium.

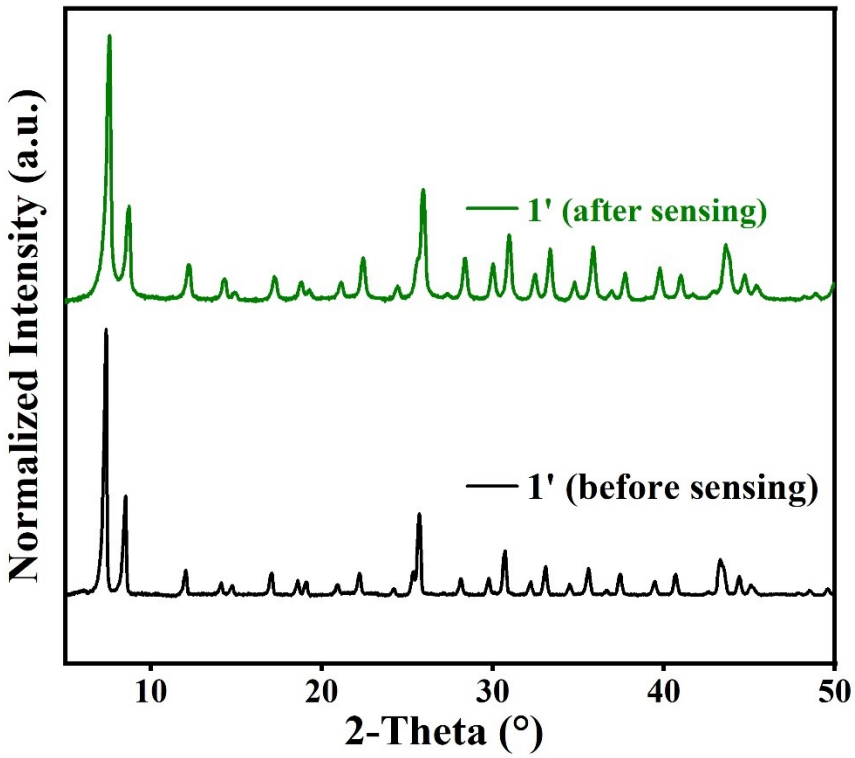

Figure S32. Comparison of PXRD profiles of **1′** before and after $[UO_2]^{2+}$ sensing in aqueous medium.

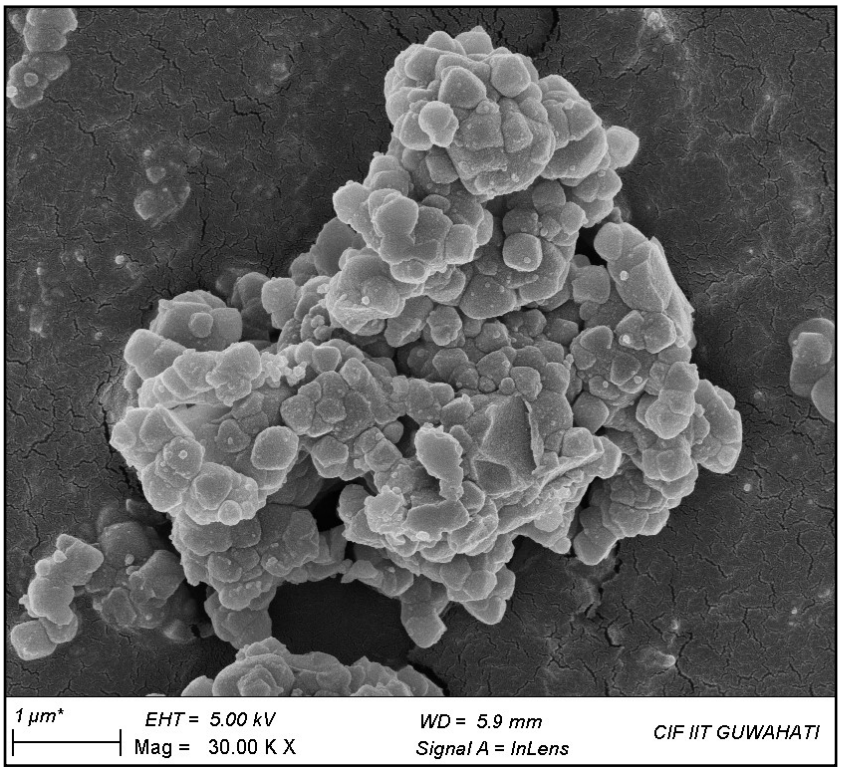

Figure S33. FE-SEM images of **1′** after sensing of $[UO_2]^{2+}$ in aqueous medium.

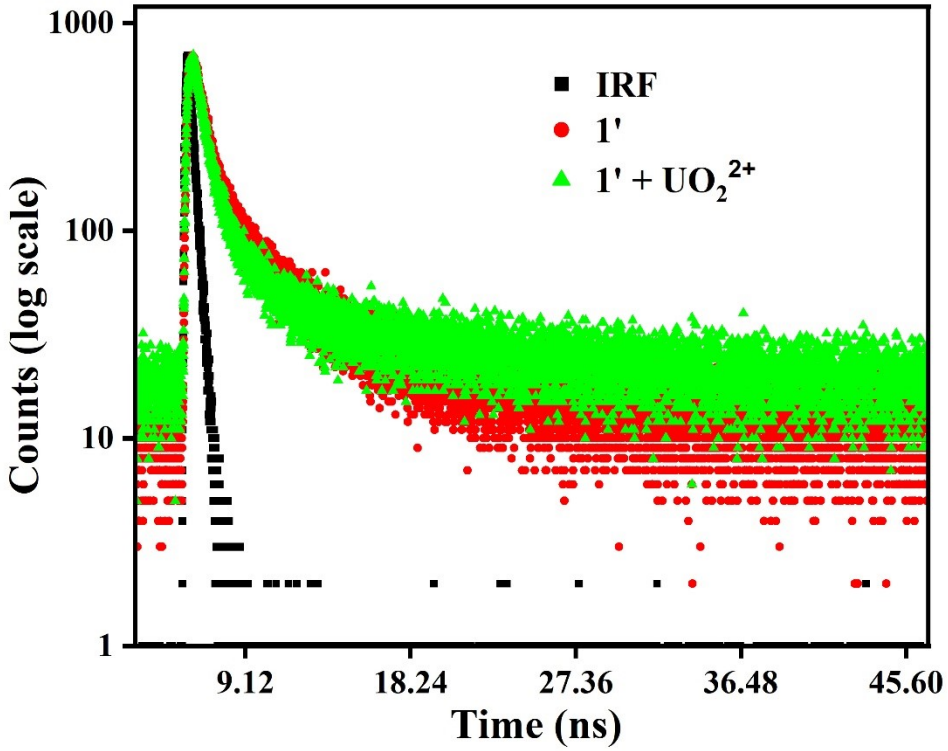

Figure S34. Lifetime decay profile of **1′** in the absence and presence of $[UO_2]^{2+}$ in aqueous solution (λ_{ex} = 310 nm, monitored at 290 nm).

Table S5. Fluorescence lifetimes of **1′** before and after the addition of $[UO_2]^{2+}$ solution (λ_{ex} = 290 nm, pulsed diode laser).

Volume of $[UO_2]^{2+}$ added (μL)	f_1	f_2	f_3	τ_1 (ns)	τ_2 (ns)	τ_2 (ns)	$<\tau>$* (ns)	χ^2
0	0.0046	0.0229	0.0011	1.49	0.29	6.43	0.71	1.07
300	0.0047	0.0008	0.0256	1.37	9.88	0.28	0.69	1.04

* $<\tau> = \Sigma f\tau/\Sigma f$

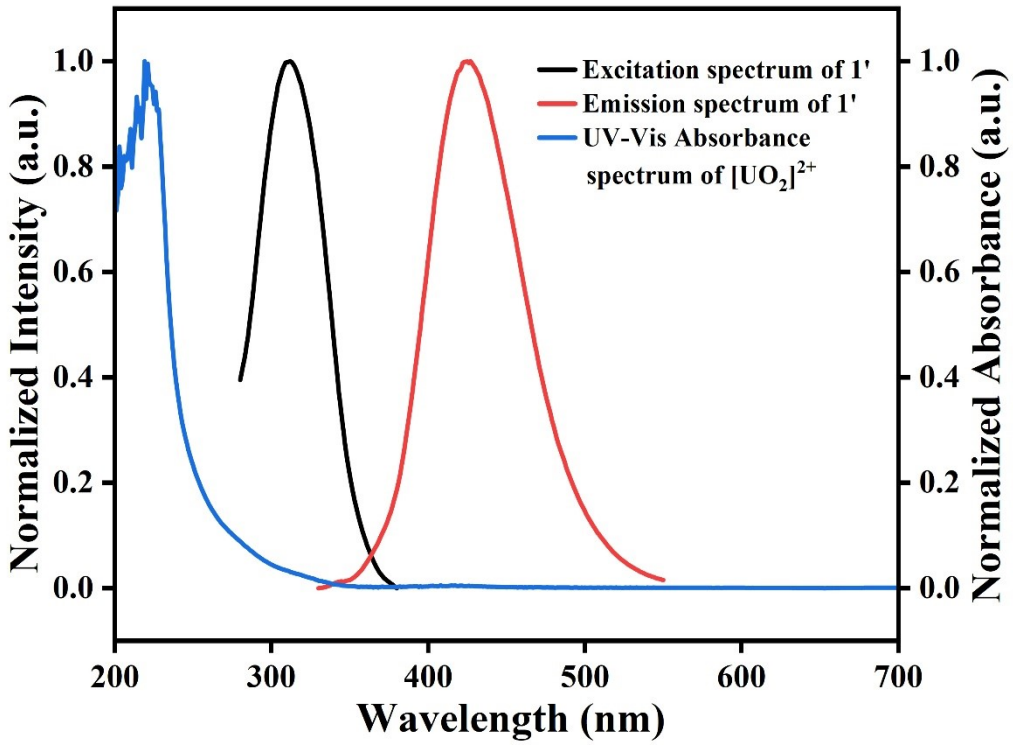

Figure S35. Spectral overlap of excitation/emission spectra of **1'** with the absorption spectrum of $[UO_2]^{2+}$.

Table S6. IFE correction table for $[UO_2]^{2+}$ sensing.

Concentration of $[UO_2]^{2+}$ (μM)	A_{ex}	A_{em}	Correction Factor (CF)	$F_{observed}$	$F_{corrected}$	$F_{corrected(0)}/F_{corrected}$
0	0.209	0.034	1.300	1260290	1638638	1
0.000	0.187	0.109	1.361	803582.018	1093958.813	1.428
32.787	0.230	0.120	1.439	389545.756	560376.497	2.788
65.359	0.237	0.130	1.463	304562.139	445502.435	3.507
97.720	0.249	0.138	1.494	256632.908	383314.040	4.076
129.870	0.256	0.141	1.509	232192.650	350359.413	4.459
161.812	0.261	0.156	1.539	212277.601	326661.375	4.783
193.548	0.278	0.163	1.576	200776.124	316501.434	4.936

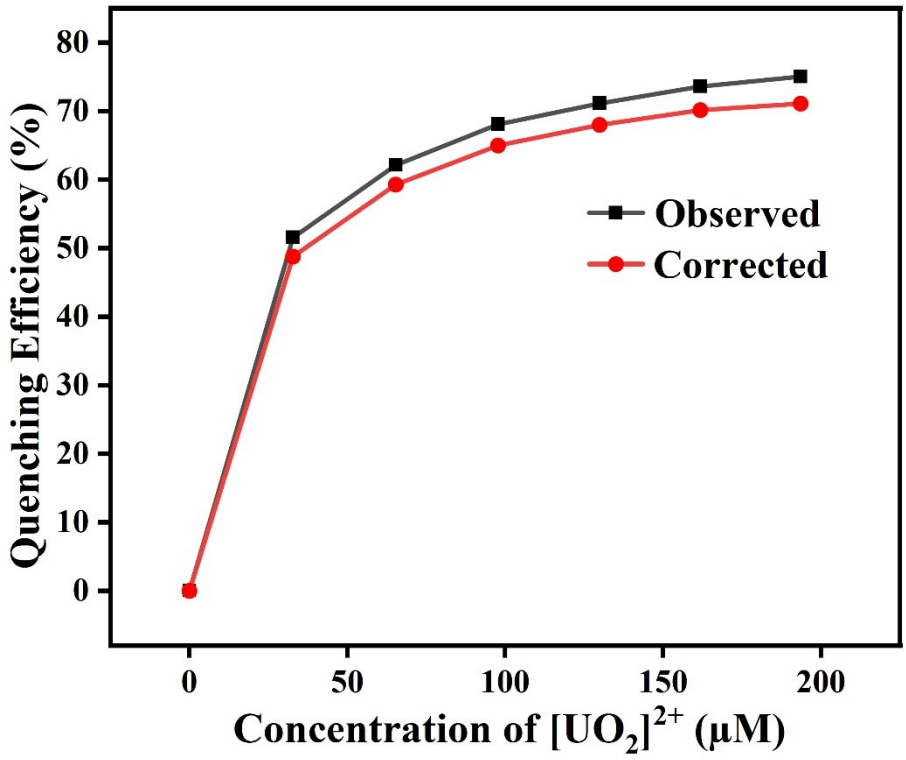

Figure S36. Observed and corrected quenching efficiency for $[UO_2]^{2+}$ sensing.

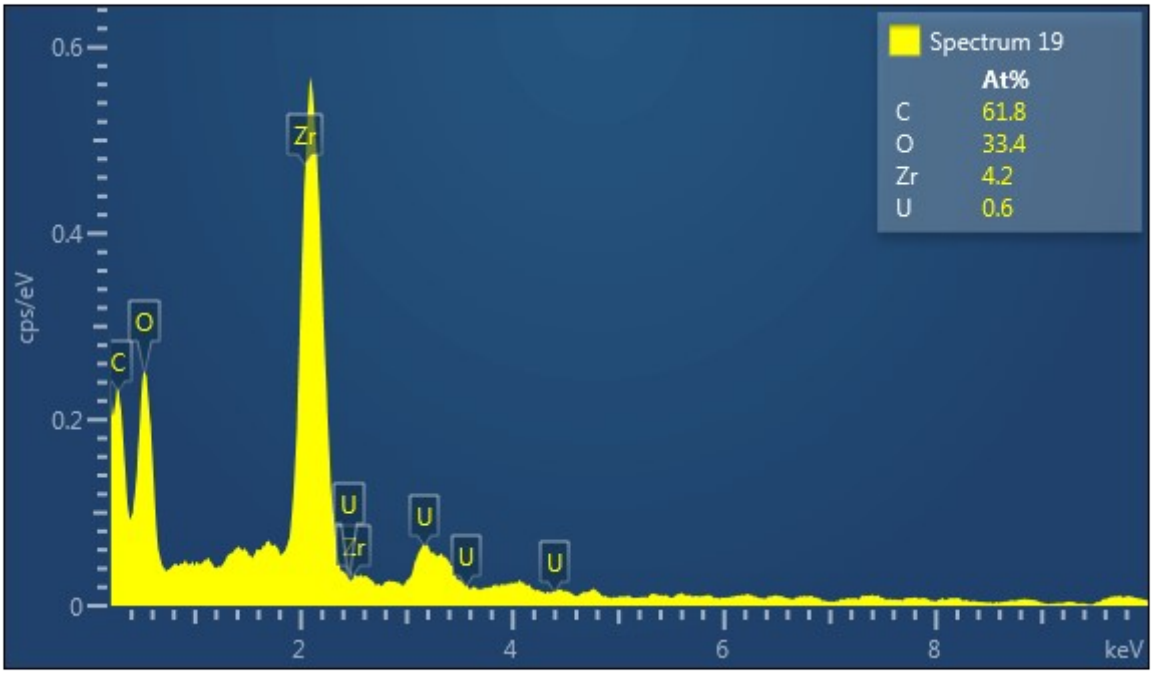

Figure S37. EDX spectrum of $[UO_2]^{2+}$ treated **1'**.

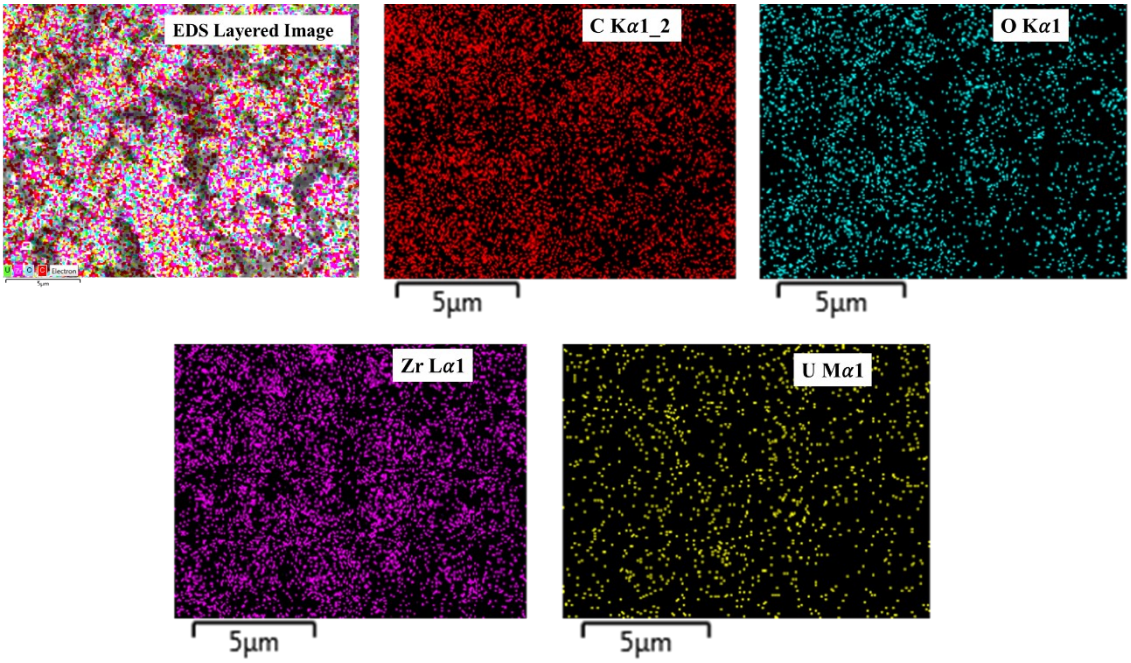

Figure S38. EDX elemental mapping of $[UO_2]^{2+}$ treated **1'**.

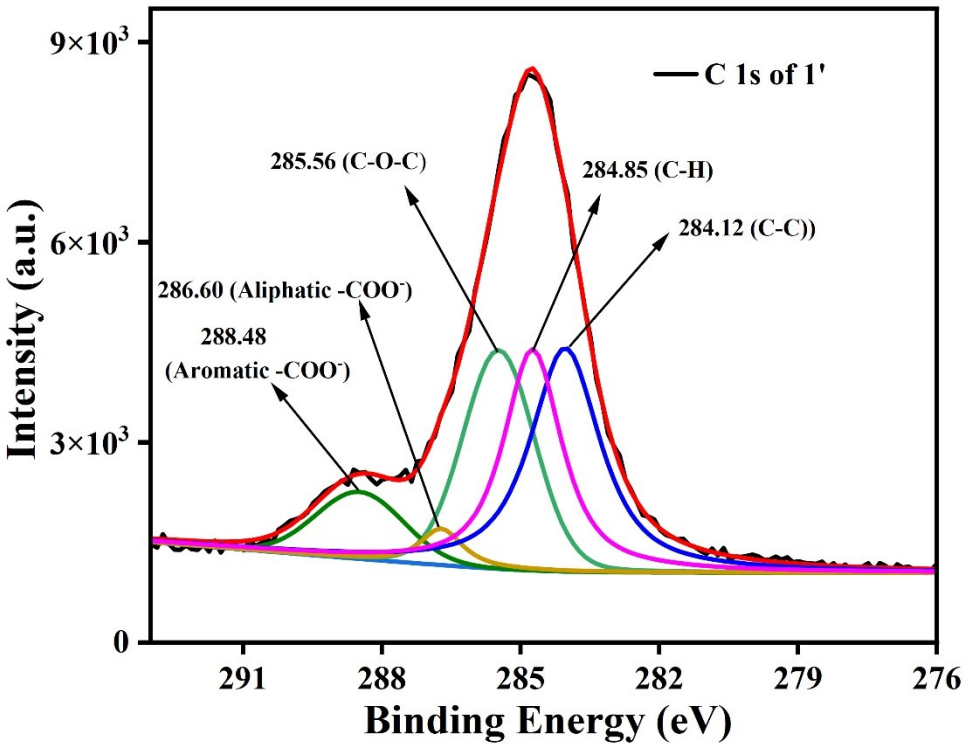

Figure S39. C 1s XPS spectrum of **1'**.

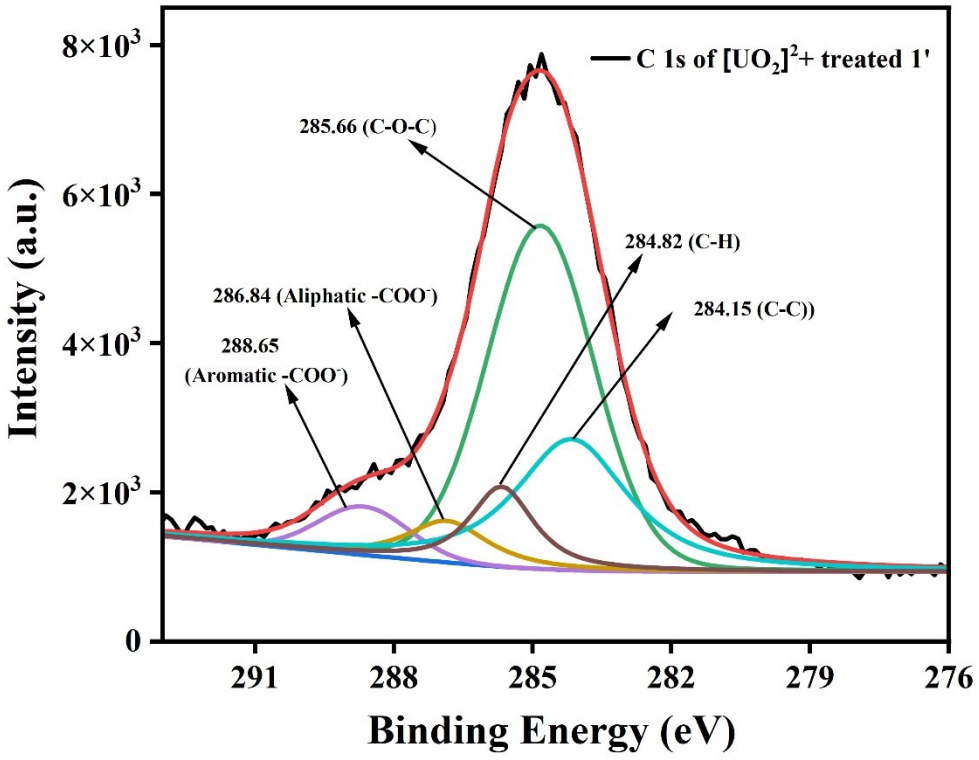

Figure S40. C 1s XPS spectrum of $[UO_2]^{2+}$ treated **1'**.

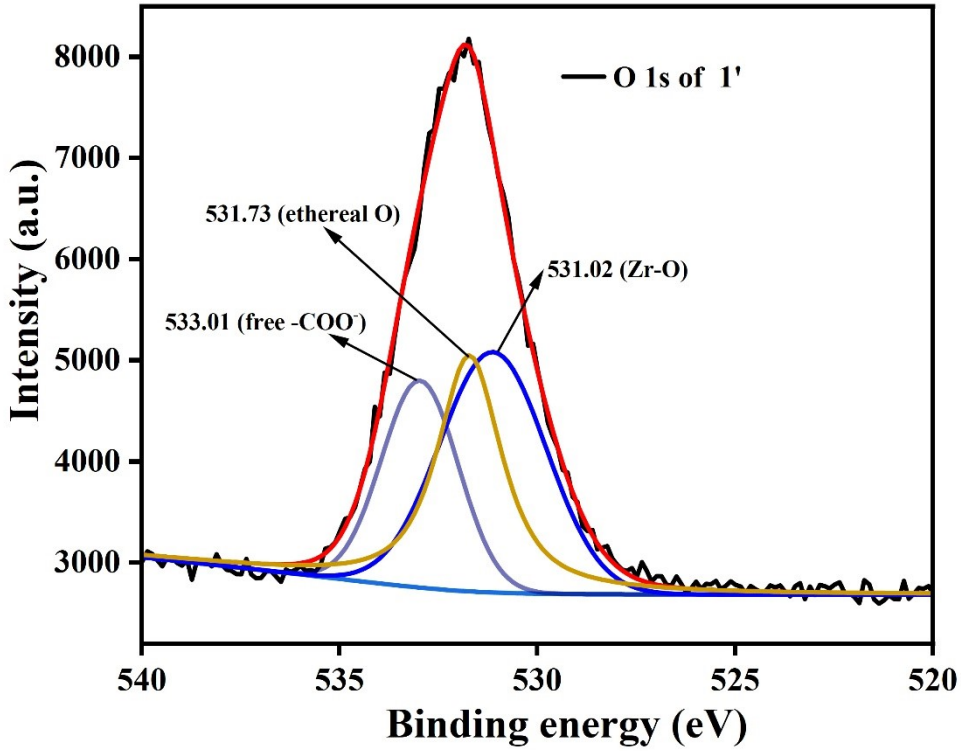

Figure S41. O 1s XPS spectrum of **1'**.

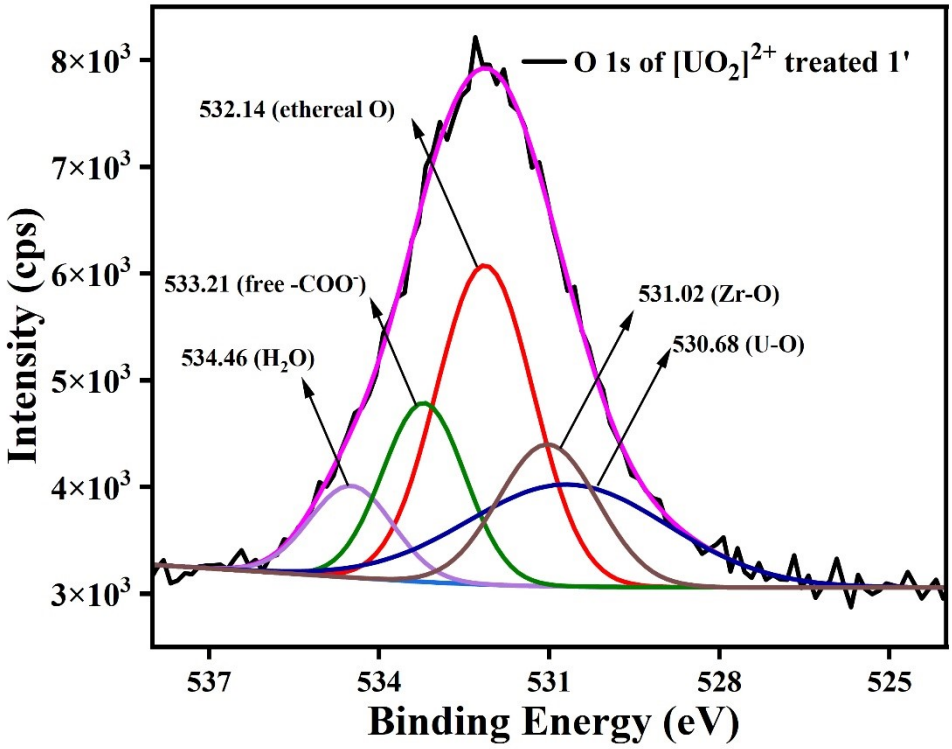

Figure S42. O 1s XPS spectrum of $[UO_2]^{2+}$ treated **1'**.

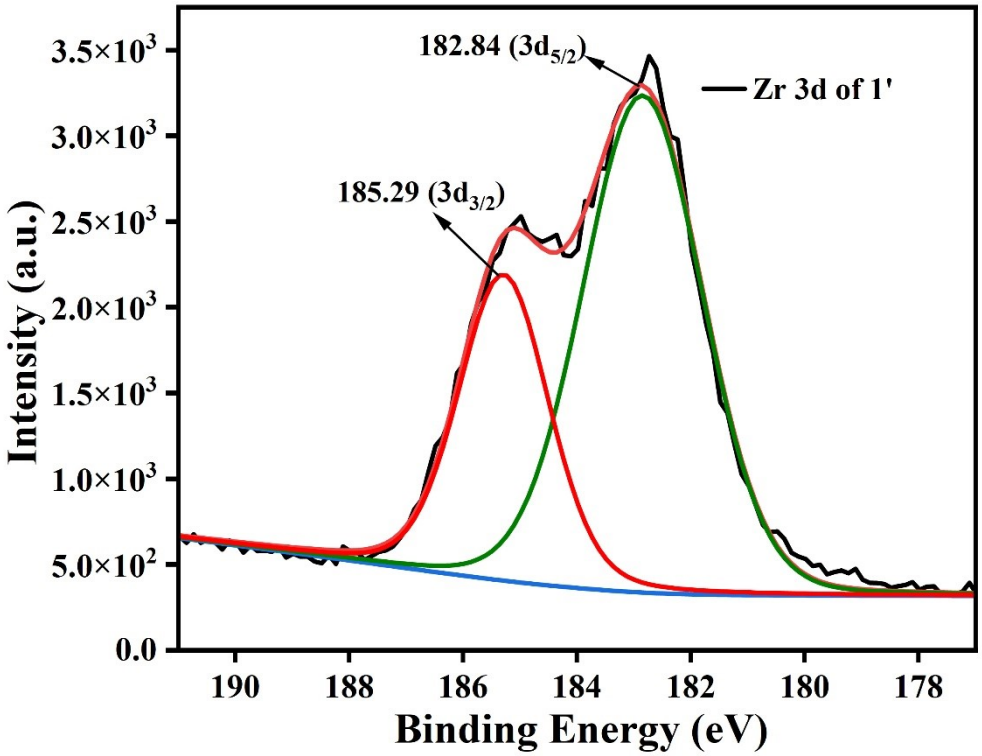

Figure S43. Zr 3d XPS spectrum of **1'**.

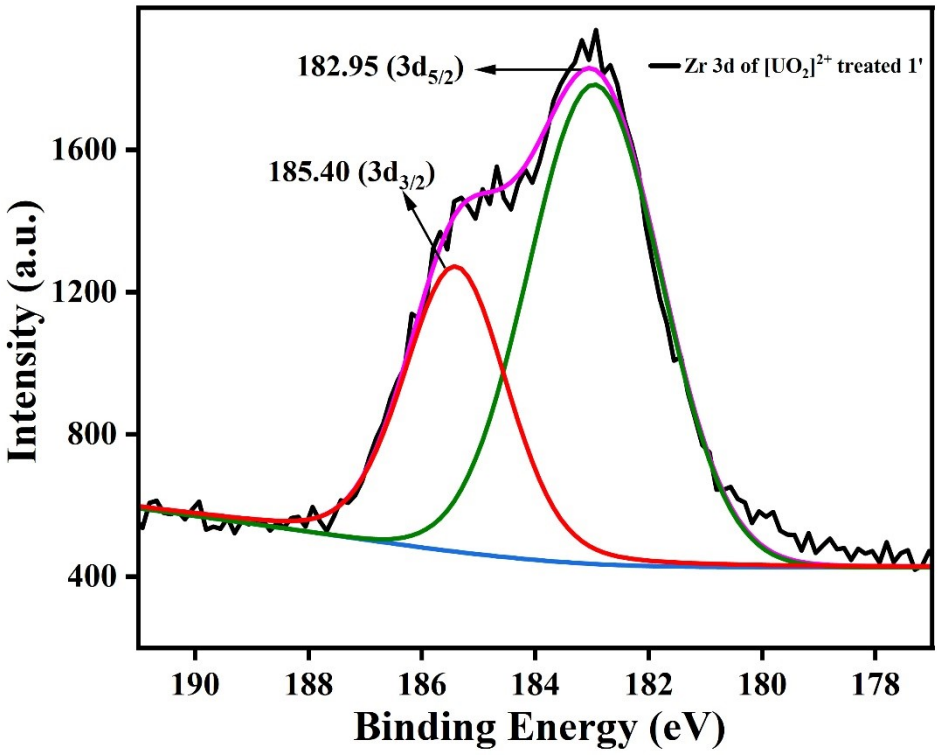

Figure S44. Zr 3d XPS spectrum of $[UO_2]^{2+}$ treated **1'**.

References:

1. Parker, C. A.; Rees, W., Correction of fluorescence spectra and measurement of fluorescence quantum efficiency. *Analyst* **1960,** *85* (1013), 587-600.
2. Biswas, S.; Vanpoucke, D. E.; Verstraelen, T.; Vandichel, M.; Couck, S.; Leus, K.; Liu, Y.-Y.; Waroquier, M.; Van Speybroeck, V.; Denayer, J. F., New functionalized metal–organic frameworks MIL-47-X (X=− Cl,− Br,− CH3,− CF3,− OH,− OCH3): synthesis, characterization, and CO2 adsorption properties. *J. Phys. Chem. C* **2013,** *117* (44), 22784-22796.
3. Samanta, P.; Desai, A. V.; Sharma, S.; Chandra, P.; Ghosh, S. K., Selective recognition of Hg2+ ion in water by a functionalized metal–organic framework (MOF) based chemodosimeter. *Inorg. Chem.* **2018,** *57* (5), 2360-2364.
4. Cavka, J. H.; Jakobsen, S.; Olsbye, U.; Guillou, N.; Lamberti, C.; Bordiga, S.; Lillerud, K. P., A new zirconium inorganic building brick forming metal organic frameworks with exceptional stability. *J. Am. Chem. Soc.* **2008,** *130* (42), 13850-13851.
5. Xie, J.; Liang, J.; Lei, J.; Xiao, Y.; Luo, F.; Hu, B., Highly Sensitive and Selective Detection of Uranyl Ions Based on a Tb^{3+}-Functionalized MOF via Competitive Host–Guest Coordination. *Inorg. Chem.* **2025,** *64* (7), 3616-3625.
6. Ye, J.; Bogale, R. F.; Shi, Y.; Chen, Y.; Liu, X.; Zhang, S.; Yang, Y.; Zhao, J.; Ning, G., A water-stable dual-channel luminescence sensor for UO_2^{2+} ions based on an anionic terbium(III) metal–organic framework. *Chem. Eur. J.* **2017,** *23* (32), 7657-7662.
7. Li, L.; Shen, S.; Su, J.; Ai, W.; Bai, Y.; Liu, H., Facile one-step solvothermal synthesis of a luminescent europium metal-organic framework for rapid and selective sensing of uranyl ions. *Anal. Bioanal. Chem.* **2019,** *411* (18), 4213-4220.

8. Lei, M.; Jia, Y.; Zhang, W.; Xie, J.; Xu, Z.; Wang, Y.; Du, W.; Liu, W., Ultrasensitive and selective detection of uranium by a luminescent terbium–organic framework. *ACS Appl. Mater. Interfaces* **2021,** *13* (43), 51086-51094.
9. Hou, J.-X.; Gao, J.-P.; Liu, J.; Jing, X.; Li, L.-J.; Du, J.-L., Highly selective and sensitive detection of Pb^{2+} and UO_2^{2+} ions based on a carboxyl-functionalized Zn(II)-MOF platform. *Dyes and Pigments* **2019,** *160*, 159-164.
10. Chen, W.-M.; Meng, X.-L.; Zhuang, G.-L.; Wang, Z.; Kurmoo, M.; Zhao, Q.-Q.; Wang, X.-P.; Shan, B.; Tung, C.-H.; Sun, D., A superior fluorescent sensor for Al^{3+} and UO_2^{2+} based on a Co(II) metal–organic framework with exposed pyrimidyl Lewis base sites. *J. Mater. Chem. A* **2017,** *5* (25), 13079-13085.
11. Chen, N. N.; Wang, J., A serial of 2D Co-Zn isomorphous metal–organic frameworks for photodegradation and luminescent detection properties. *Appl. Organomet. Chem.* **2020,** *34* (9), e5743.
12. Wang, N.; Du, J.; Li, X.; Ji, X.; Wu, Y.; Sun, Z., Magnetic MOF substrates for the rapid and sensitive surface-enhanced Raman scattering detection of uranyl. *Anal. Chem.* **2023,** *95* (34), 12956-12963.